


## Energetic and entropic cost due to overlapping of Turing-Hopf instabilities in the presence of cross diffusion

Premashis Kumar  and Gautam Gangopadhyay *S. N. Bose National Centre For Basic Sciences, Block-JD, Sector-III, Salt Lake, Kolkata 700 106, India* (Received 26 September 2019; accepted 28 February 2020; published 9 April 2020)

A systematic introduction to nonequilibrium thermodynamics of dynamical instabilities are considered for an open nonlinear system beyond conventional Turing pattern in presence of cross diffusion. An altered condition of Turing instability in presence of cross diffusion is best reflected through a critical control parameter and wave number containing both the self- and cross-diffusion coefficients. Our main focus is on entropic and energetic cost of Turing-Hopf interplay in stationary pattern formation. Depending on the relative dispositions of Turing-Hopf codimensional instabilities from the reaction-diffusion equation it clarifies two aspects: energy cost of pattern formation, especially how Hopf instability can be utilized to dictate a stationary concentration profile, and the possibility of revealing nonequilibrium phase transition. In the Brusselator model, to understand these phenomena, we have analyzed through the relevant complex Ginzburg-Landau equation using multiscale Krylov-Bogolyubov averaging method. Due to Hopf instability it is observed that the cross-diffusion parameters can be a source of huge change in free-energy and concentration profiles.

DOI: [10.1103/PhysRevE.101.042204](https://doi.org/10.1103/PhysRevE.101.042204)

### I. INTRODUCTION

The traditional Turing pattern [1–5] with very different self-diffusion coefficients and traveling waves [6–8] are prevalent in the living tissues as morphogens [9–12], in cellular rhythms [13–15], and in many such situations [16–18]; however, a reaction-diffusion system can be drastically modified due to the slight presence of cross diffusion which is still underinvestigated [19–21]. Thermodynamics of pattern formation, or, more generally, far from the equilibrium system, is addressed at length in the literature starting from the description of dissipative energy loss [22,23] to stochastic thermodynamics [24,25], along with thermal transport problems [26,27] and demonstrations of the validity of fluctuation theorems [28,29], paving the way to a systematic calculation of thermodynamic quantities in open dynamical systems. From a theoretical point of view it is still challenging to develop an approach to deal with an arbitrary nonlinear nonequilibrium process to tackle the problems of complex chemical network [30,31] in a heterogeneous medium. Our goal here is to develop theories of non-equilibrium consequences of various dynamical instabilities in open systems describable as a reaction-diffusion system. Particularly the dynamical characterization of inbuilt limit-cycle oscillation in the presence of cross-diffusion coefficients resulting from diffusive flux of one species due to gradient in concentration of another [16] takes its toll by altering their bifurcation scenario.

Whenever a closed system is opened by chemostatting, either a subset of conservation laws are broken or an emergent cycle appears for each chemostatted species [30]. If there is no emergent cycle for open chemical reaction network

with homogeneous chemostatting, then the system is said to be unconditionally detailed balanced for a finite number of species and reactions due to absence of any nonconservative forces [31]. In open reaction-diffusion system, Gibbs free energy is not minimized due to the breaking of conservation laws which is characterized for closed system. Analogously to the definition of grand potential in terms of the Gibbs free energy in equilibrium thermodynamics, the semigrand Gibbs free energy of the open system can be defined from the nonequilibrium Gibbs free energy of the system by subtracting the energetic contribution due to exchange of matter between chemostats and system [32]. In the reaction-diffusion system, the amplitude equation [33] is already used to capture a large degree of richness of pattern formation both qualitatively and quantitatively near the onset of the instability [1]. To treat the generic nonlinear dynamics with symmetries and bifurcation characteristics of the system one can find the description of multiscale perturbation theory to obtain the amplitude equation [17,33,34] in terms of the complex Ginzburg Landau equation (CGLE).

In this context quantifying entropic and energetic costs of various pattern formation and interplay of various nonlinearity-induced instabilities are of crucial theoretical concern here. This kind of approach has been adopted recently to study the thermodynamics of the Turing pattern in the presence of self-diffusion only [35] and chemical waves [36]. Again, mathematical analysis of Turing-Hopf interplay has got some attention in different dynamical contexts [37–40], but a thermodynamic description of the overlap of Turing-Hopf instabilities is still missing. Moreover, in the study of pattern formation, very often cross-diffusion coefficients of the species have been ignored; however, they can have a very significant effect to modify almost all the patterns even if they are minimal [41]. In reaction-diffusion system corresponding

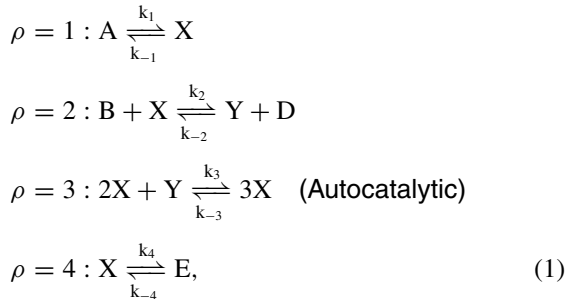
\*gautam@bose.res.in

to traditional Turing pattern, threshold of Turing and Hopf instabilities are well separated for very different diffusion coefficients of activator and inhibitor. Proper choice of cross-diffusion coefficients can bring the threshold of Turing and Hopf instabilities close enough so that they eventually overlap and as a consequence a large variety of complex spatiotemporal patterns are likely to emerge beyond a critical Turing-Hopf point. As the usual multiscale methods [1,17] of deriving the amplitude equation, especially for the reaction-diffusion system with cross diffusion, is rather cumbersome, and we have employed here a simple method of derivation based on the Krylov-Bogolyubov (KB) averaging method [42] to obtain the relevant Ginzberg-Landau equation.

The layout of the paper is as follows. In Sec. II we discuss the chemostatted Brusselator model with cross diffusion. Turing and Hopf instabilities are estimated for this system in the next section. In Sec. IV we have derived the amplitude equation using the Krylov-Bogolyubov method. Entropy production rate is calculated for the reaction-diffusion system in Sec. V. In the next section, the nonequilibrium Gibbs free energy of chemostatted system is formulated. In Sec. VII concentration fields of the intermediate species are obtained using analytical approach. We have provided numerical results and discussions in Sec. VIII. Finally, the paper is concluded in Sec. IX.

## II. BRUSSELATOR MODEL WITH CROSS DIFFUSION

The Brusselator model [22,23] is a prototype for studying various cooperative behavior in chemical kinetics and can successfully mimic the oscillatory Belousov-Zhabotinsky (BZ) reaction [43]. The reversible Brusselator model contains the following sequence of chemical reactions:



where  $\rho$  is a reaction step label,  $\{X, Y\} \in I$  are two intermediate species having dynamic concentration, and  $\{A, B, D, E\} \in C$  are initial and final products with a constant homogeneous concentration along the entire system within the timescale of interest. Main features of the Brusselator model as an open chemical reaction network are presented in Fig. 1.

The stoichiometric matrix of the Brusselator reaction network in Eq. (1) is

$$S_{\rho}^{\sigma} = \begin{matrix} & R_1 & R_2 & R_3 & R_4 \\ \begin{matrix} X \\ Y \\ A \\ B \\ D \\ E \end{matrix} & \begin{pmatrix} 1 & -1 & 1 & -1 \\ 0 & 1 & -1 & 0 \\ -1 & 0 & 0 & 0 \\ 0 & -1 & 0 & 0 \\ 0 & 1 & 0 & 0 \\ 0 & 0 & 0 & 1 \end{pmatrix} \end{matrix}. \tag{2}$$

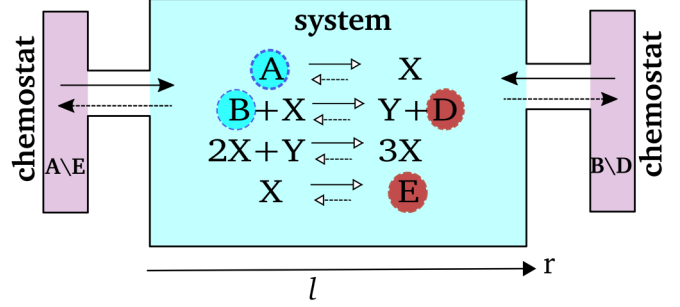


FIG. 1. Illustration of the Brusselator model as an open chemical network where A and B are reference chemostatted species. One can also use D and E as reference chemostatted species. Reservoirs of chemostatted species are shown in the two sides (purple) and finite system of length  $l$  is shown in the middle (sky blue).

With the assumptions, all the reverse rate constants  $k_{-\rho}$  are vanishingly small ( $10^{-4}$ ), and the forward reaction rate constants  $k_{\rho}$  are much higher than the reverse one, i.e.,  $k_{\rho} \gg k_{-\rho}$ , the rate equations of concentrations of intermediate species in Eq. (1) read as

$$\begin{aligned}
 \dot{x} &= k_1 a - (k_2 b + k_4)x + k_3 x^2 y \\
 \dot{y} &= k_2 b x - k_3 x^2 y,
 \end{aligned} \tag{3}$$

where concentration of species are denoted by lowercase letters,

$$x = [X], \quad y = [Y], \quad b = [B], \quad a = [A].$$

The steady-state value of the Eq. (3) that satisfies  $\dot{x} = \dot{y} = 0$  is  $x_0 = \frac{k_1 a}{k_4}$  and  $y_0 = \frac{k_2 k_4 b}{k_1 k_3 a}$ .

Now after taking diffusion into account, the reaction-diffusion equation of the Brusselator model in one spatial dimension  $r \in [0, l]$  could be specified as

$$\begin{aligned}
 \dot{x} &= k_1 a - (k_2 b + k_4)x + k_3 x^2 y + D_{11} x_{rr} + D_{12} y_{rr} \\
 \dot{y} &= k_2 b x - k_3 x^2 y + D_{21} x_{rr} + D_{22} y_{rr},
 \end{aligned} \tag{4}$$

in which  $D_{11}, D_{22}$  are self-diffusion coefficients of intermediate species X and Y, respectively, and  $D_{12}, D_{21}$  are cross-diffusion coefficients of X and Y, respectively.

This cross-diffusion coefficients generally have concentration dependence [41]. Most importantly, the vanishingly low concentration of the species,  $\sigma$ , demands no flux of the species  $\sigma$  ( $\sigma = 1, 2, \dots$ ). Therefore cross-diffusion coefficients  $D_{\sigma\sigma'} (\sigma \neq \sigma')$  must tend to vanish as the concentration  $z_{\sigma}$  tends to zero irrespective of the gradient in the concentration,  $z_{\sigma}'$ . Following the work of Chung and Peacock-Lopez [44], we can represent the concentration dependence of the cross-diffusion coefficients as the

$$D_{\sigma\sigma'}(z_{\sigma}) = \frac{D_{\sigma\sigma'} z_{\sigma}}{\eta + z_{\sigma}}. \tag{5}$$

According to Eq. (5), for  $z_{\sigma} = 0$ ,  $D_{\sigma\sigma'}$  will always vanish and thus, it satisfies the demand mentioned above. Moreover, for the minimal value of the  $\eta$  with respect to concentrations i.e.,  $\eta \ll z_{\sigma}$ ,  $D_{\sigma\sigma'}(z_{\sigma})$  will be merely equal to the constant  $D_{\sigma\sigma'}$ . Whereas if the constant  $\eta$  is very large compare to concentrations, i.e.,  $\eta \gg z_{\sigma}$ , then  $D_{\sigma\sigma'}(z_{\sigma}) = \frac{D_{\sigma\sigma'} z_{\sigma}}{\eta} = D'_{\sigma\sigma'} z_{\sigma}$  with

$D'_{\sigma\sigma'} = \frac{D_{\sigma\sigma'}}{\eta}$  and thus cross-diffusion coefficients have linear concentration dependence. For simplicity, we have considered here the case ( $\eta \ll z_i$ ) of constant cross-diffusion coefficients for the most of the analysis for dynamic and thermodynamic entities in the Brusselator model.

### III. TURING AND HOPF INSTABILITIES AND THE BRUSSLATOR MODEL

In the reaction-diffusion system, one can have both Hopf and Turing instabilities which can be obtained from linear stability analysis. Evolution equations of the reaction-diffusion system can be found by considering single Fourier mode of the form  $\exp[\lambda(q)t + iqr]$  where growth rate has wave number  $q$  dependence. For linear stability analysis at the steady-state value  $(x_0, y_0)$ , one needs the Jacobian matrix of the Brusselator model,

$$\mathcal{J} = \begin{bmatrix} -(k_2b + k_4) + 2k_3x_0y_0 & k_3x_0^2 \\ k_2b - 2k_3x_0y_0 & -k_3x_0^2 \end{bmatrix}. \quad (6)$$

Here elements of the Jacobian matrix,  $\mathcal{J}$ , are the following:

$$J_{11} = -(k_2b + k_4) + 2k_3x_0y_0, J_{12} = k_3x_0^2 \\ J_{21} = k_2b - 2k_3x_0y_0, J_{22} = -k_3x_0^2.$$

In this context it is to be noted that the Oregonator model [45,46] is the simplest model for describing the oscillations in BZ reaction having Jacobian with a sign structure (pure activator-inhibitor) opposite to that of the Brusselator model (cross activator-inhibitor).

#### A. Turing instability

When the cross-diffusion coefficients are present in the system and contribute to the Turing pattern, then the self-diffusion coefficients do not need to obey the condition of local activation and lateral inhibition [9]. Kumar and Horsthemke showed that presence of cross diffusion strongly modifies the Turing instability conditions and in this case Turing instability can arise even if the self-diffusion coefficient of the inhibitor is more than the self-diffusion of the activator [19]. Zemskov *et al.* have presented universal conditions of the Turing instability in the presence of the cross-diffusion coefficients with a linear concentration dependence. With the aid of those conditions, they have described the proper Turing instability region [20]. Lin *et al.* have investigated the influence of cross diffusion in selecting the spatial pattern for the Busselator model in a three-dimensional domain [21]. By using the finite-volume-element approximation, they have shown that cross diffusion can generate a Turing pattern in this three-dimensional case. Exploiting conditions of Turing instability in the presence of cross diffusion, one can obtain a critical value of the control parameter and wave number. We would next find out those critical values in the 1D Brusselator model in the presence of both self- and cross-diffusion coefficients.

In the presence of diffusion, Jacobian  $\mathcal{J}$  becomes

$$\mathcal{J}_{\mathcal{D}} = \mathcal{J} - q^2\mathcal{D} \\ = \begin{bmatrix} -(k_2b + k_4) + 2k_3x_0y_0 & k_3x_0^2 \\ k_2b - 2k_3x_0y_0 & -k_3x_0^2 \end{bmatrix} - q^2 \begin{pmatrix} D_{11} & D_{12} \\ D_{21} & D_{22} \end{pmatrix}, \quad (7)$$

where we have applied a Fourier transform  $g(r, t) \rightarrow g(q, t)$ , with  $q$  being the wave number. Now the trace of the  $\mathcal{J}_{\mathcal{D}}$  will be simply:  $\text{Tr}(\mathcal{J}_{\mathcal{D}}) = \text{Tr}(\mathcal{J}) - q^2\text{Tr}(\mathcal{D}) = k_2b - k_4 - \frac{k_3k_1^2}{k_4}a^2 - (D_{11} + D_{22})q^2$  and determinant of  $\mathcal{J}_{\mathcal{D}}$  will be

$$\det(\mathcal{J}_{\mathcal{D}}) = \det(\mathcal{D})q^4 - [D_{11}J_{22} + D_{22}J_{11} - D_{12}J_{21} \\ - D_{21}J_{12}]q^2 + \det(\mathcal{J}), \quad (8)$$

a quadratic equation of  $q^2$  in which  $\det(\mathcal{J}) = \frac{k_1^2k_3}{k_4}a^2$  is determinant of  $\mathcal{J}$ . Eigenvalues  $\lambda$  of  $\mathcal{J}_{\mathcal{D}}$  are given by the characteristic equation

$$\lambda^2 - \text{Tr}(\mathcal{J}_{\mathcal{D}})\lambda + \det(\mathcal{J}_{\mathcal{D}}) = 0.$$

Hence eigenvalues can be expressed only in terms of determinant and trace as

$$\lambda_{\pm} = \frac{\text{Tr}(\mathcal{J}_{\mathcal{D}}) \pm \sqrt{\text{Tr}(\mathcal{J}_{\mathcal{D}})^2 - 4\det(\mathcal{J}_{\mathcal{D}})}}{2}. \quad (9)$$

Stability criterion simply demands both of these eigenvalues have to be negative and thus, in terms of trace and determinant, this implies  $\text{Tr}(\mathcal{J}_{\mathcal{D}}) < 0$  and  $\det(\mathcal{J}_{\mathcal{D}}) > 0$ . As chemical concentrations are real quantities, eigenvalues are complex conjugate pair  $\lambda_{\pm} = \lambda_r \pm i\lambda_i$  at stable steady state. Since the system was at stable steady state before adding diffusion with  $[(D_{11} + D_{22})q^2] > 0$  being always true, trace condition of stability,  $\text{Tr}(\mathcal{J}_{\mathcal{D}}) < 0$ , remains intact even in the presence of the diffusion. So the only way to have diffusion-driven instability is by breaking the determinant condition of stability in the presence of diffusion. Therefore,  $\det(\mathcal{J}_{\mathcal{D}}) < 0$  in the instability regime and at the onset of Turing instability,  $\det(\mathcal{J}_{\mathcal{D}}) = 0$ . Now, from the second law of thermodynamics,  $\det(\mathcal{D}) > 0$  is always true and the existence of stable steady state in the absence of diffusion demands  $\det(\mathcal{J}) > 0$ . So the only way to satisfy the  $\det(\mathcal{J}_{\mathcal{D}}) < 0$  condition is

$$[D_{11}J_{22} + D_{22}J_{11}] > [D_{12}J_{21} + D_{21}J_{12}]. \quad (10)$$

The above condition implies one of the eigenvalues crosses zero to become positive and is a necessary but not sufficient condition to have Turing instability in the presence of cross diffusion. From the necessary condition stated in Eq. (10), it appears that in the presence of cross diffusion, so-called local activation, and lateral inhibition for a traditional Turing pattern need not be followed. To obtain the necessary and sufficient condition for having a Turing instability-induced spatial pattern, we need to ensure the existence of the real root of quadratic Eq. (8), i.e., to satisfy the following condition:

$$(D_{11}J_{22} + D_{22}J_{11} - D_{12}J_{21} - D_{21}J_{12})^2 - 4\det(\mathcal{D})\det(\mathcal{J}) > 0. \quad (11)$$

If we assume that by varying the control parameter,  $b$ , the onset of instability is reached, then the condition in Eq. (11) simply results in the following equality:

$$(D_{11}J_{22} + D_{22}J_{11} - D_{12}J_{21} - D_{21}J_{12})^2 - 4\det(\mathcal{D})\det(\mathcal{J}) = 0. \quad (12)$$

Inserting all the elements of Jacobian,  $\mathcal{J}$ , and  $\det(\mathcal{J})$  into Eq. (12), we will find the critical value of the bifurcation

parameter in the Brusselator model as

$$b_{cT} = \left( \frac{[D_{11} \frac{k_1^2 k_3}{k_4^2} + D_{21} \frac{k_1^2 k_3}{k_4^2}] a^2 + 2[\det(\mathcal{D})]^{\frac{1}{2}} [\frac{k_1^2 k_3}{k_4}]^{\frac{1}{2}} a + D_{22} k_4}{D_{22} k_2 + D_{12} k_2} \right). \tag{13}$$

Eigenvalues at the onset of Turing instability now becomes

$$\lambda_+ = \text{Tr}(\mathcal{J}_D) = k_2 b_{cT} - k_4 - \frac{k_3 k_1^2}{k_4^2} a^2 - (D_{11} + D_{22}) q_{cT}^2$$

and  $\lambda_- = 0$ . Here  $q_{cT}$  is an intrinsic critical wave number and  $b_{cT}$  is critical value of the control parameter at the onset of Turing instability. Negative value of the  $\text{Tr}(\mathcal{J}_D)$  means that eigenvalue  $\lambda_- = 0$  at the Turing instability will govern the whole dynamics of the system.

The necessary and sufficient condition to have Turing instability is that the  $\det(\mathcal{J}_D)$  equation must have double roots at the onset of instability, i.e., the following two conditions are satisfied simultaneously:  $\det(\mathcal{J}_D) = 0$  and  $\frac{d(\det(\mathcal{J}_D))}{d(q^2)} = 0$ . This will result in the equation of intrinsic critical wave number at the onset of instability,

$$q_{cT} = \left[ \frac{\det(\mathcal{J})}{\det(\mathcal{D})} \right]^{\frac{1}{4}} = \left[ \frac{k_1^2 k_3}{k_4} \frac{a^2}{\det(\mathcal{D})} \right]^{\frac{1}{4}} \tag{14}$$

and it will set the length scale as  $\frac{2\pi}{q_{cT}}$ . This  $q_{cT}$  is the fastest-growing Fourier mode and for the critical value of the control parameter the growth rate first becomes zero at this critical wave number. Now for Turing instability the critical eigenvector,  $U_{cT}$ , corresponding to eigenvalue  $\lambda_{q_{cT}} = 0$  is

$$U_{cT} = \begin{bmatrix} 1 \\ -\frac{k_4}{(D_{12}+D_{22})q_{cT}^2} - \frac{(D_{21}+D_{11})}{(D_{12}+D_{22})} \end{bmatrix} = \begin{bmatrix} 1 \\ -\frac{k_4}{k_1} \sqrt{\frac{k_4}{k_3}} \frac{\sqrt{\det(\mathcal{D})}}{(D_{12}+D_{22})a} - \frac{(D_{21}+D_{11})}{(D_{12}+D_{22})} \end{bmatrix}. \tag{15}$$

Above the critical parameter value, a quite small but finite band of Fourier modes in the vicinity of the critical wave number,  $q_{cT}$ , is considered to be equally excited and thus contributes to nonlinear growth of the spatial pattern. However, in a finite system with length  $l$  subjected to the zero flux boundary condition, the accessible critical wave number will be given by  $q_{cT} = \frac{n\pi}{L}$  for Turing instability. One needs to set the integer value,  $n$ , in such a way that the admissible critical wave number is nearest to the intrinsic critical wave number,  $q_{cT}$ .

The circumstances for Turing instability in the Brusselator are more favorable if  $D_{21}$  is negative and  $D_{12}$  is positive [19,20]. However, too much negative  $D_{21}$  or positive  $D_{12}$  values may suppress the Turing instability in the Brusselator model [19]. The conditions in cross-diffusion coefficients to obtain favorable circumstances of Turing instability will be inverted in the case of the model like Oregonator because of the opposite cross-kinetic behavior compared to the Brusselator model.

### B. Hopf instability

Besides diffusion-driven Turing instability, reaction-diffusion system could also have a type III-o ([1], ch. 10) oscillatory Hopf instability with critical wave number  $q_{cH} = 0$ . For Hopf instability as the control parameter is varied, the trace condition of the stability will be broken as  $\text{Tr}(\mathcal{J}_D)|_{q=0}$  moves to the positive value, but the initial determinant condition holds. So at the onset of Hopf instability,  $\text{Tr}(\mathcal{J}_D)|_{q=0} = 0$ , i.e.,  $J_{11} + J_{22} = 0$  or  $J_{11} = -J_{22}$  and this condition leads to critical value of control parameter as

$$b_{cH} = \frac{k_4}{k_2} + \frac{k_1^2 k_3}{k_2 k_4^2} a^2. \tag{16}$$

Real parts of complex conjugate eigenvalues which are negative initially will be zero at  $b = b_{cH}$  and eigenvalues can be expressed only in terms of determinant of the Jacobian matrix following from Eq. (9) as

$$\lambda_{\pm} = \pm i \sqrt{\det(\mathcal{J}_D)|_{q=0}} = \pm i \sqrt{\frac{k_1^2 k_3}{k_4}} a. \tag{17}$$

The critical frequency of Hopf bifurcation,  $\omega_{cH}$ , is given by the imaginary part of the eigenvalue at the onset of instability. Therefore, the period of the limit cycle near the the Hopf instability, i.e., slightly above  $b_{cH}$ , is approximately  $T = \frac{2\pi}{\omega_{cH}}$ , where  $\omega_{cH} = \sqrt{\frac{k_1^2 k_3}{k_4}} a$  for the Brusselator model. The critical eigenvector,  $U_{cH}$ , corresponding to the eigenvalue  $\lambda = i\sqrt{\det(\mathcal{J})}$  at the onset of Hopf instability in the Brusselator model is

$$U_{cH} = \begin{bmatrix} 1 + i \frac{\sqrt{\det(\mathcal{J})}}{J_{11}} \\ \frac{J_{21}}{J_{11}} \end{bmatrix} = \begin{bmatrix} 1 + \frac{i}{a} \sqrt{\frac{k_4}{k_3}} \frac{1}{k_1} \\ -(1 + \frac{k_4^3}{k_3 k_1^2} \frac{1}{a^2}) \end{bmatrix}. \tag{18}$$

### IV. DERIVATION OF AMPLITUDE EQUATION USING THE KRYLOV-BOGOLYUBOV METHOD

Amplitude is a complex entity that often features characteristics analogous to those of the order parameter in phase transition [33], and its profile in pattern formation shows a pitchfork bifurcation in a system with translational symmetry. Turing and Hopf interplay, and their relative strength and stability can be studied by exploiting the analytic solutions of their respective amplitude equations.

The KB averaging method is a standard method for analysis of oscillation in nonlinear mechanics [42]. The essential idea of this averaging method consists of varying the magnitude and phase of the amplitude so slowly in time and space that the solution of the averaged system approximates the exact dynamics. Introducing two new variables, namely the total concentration of internal species,  $z = x - y$  and  $u = a - x$ , it is possible to rewrite Eq. (3) of the Brusselator model. Substitution of new variables and with simplification of all

the forward rate constants setting as unity, the steady-state solution is given by  $u_s = 0$  and  $z_s = \frac{b}{a} + a$ . To shift the fixed point into the origin a new variable  $\zeta = z - z_s$  has been introduced to obtain a single second-order equation with a form quite similar to that of the generalized Rayleigh equation [47,48] as

$$\ddot{\zeta} + \Omega^2 \zeta = \lambda[2(1 + c_1 u - c_2 u^2)u - \frac{1}{\lambda}(u^2 - 2\Omega u)\zeta], \quad (19)$$

where  $\Omega = a$ ,  $\lambda = \frac{b-1-a^2}{2}$ , and  $c_1 = \frac{(2a-\frac{b}{a})}{2\lambda}$ ,  $c_2 = \frac{1}{2\lambda}$ .

Now by taking  $2(1 + c_1 u - c_2 u^2)u - \frac{1}{\lambda}(u^2 - 2\Omega u)\zeta = h$  Eq. (19) becomes

$$\ddot{\zeta} + \Omega^2 \zeta = \lambda h. \quad (20)$$

Now in the presence of the both self- and cross-diffusion coefficients, which are in general unequal, we can write Eq. (20) in the following form:

$$\begin{aligned} \ddot{\zeta} + \Omega^2 \zeta = \lambda h + (D_{22} + D_{12} - D_{11} - D_{21})\dot{u}_{rr} \\ + (D_{22} + D_{12})\dot{\zeta}_{rr} + (D_{11} - D_{12})u_{rr} - D_{12}\zeta_{rr}. \end{aligned} \quad (21)$$

For a very small value of  $\lambda$ , Eq. (21) admits simple harmonic functionlike solutions,

$$\zeta(r, t) = \mathcal{A}(r, t) \cos[\Omega t - \phi(r, t)], \quad (22a)$$

$$u(r, t) = \dot{\zeta}(r, t) = -\Omega \mathcal{A}(r, t) \sin[\Omega t - \phi(r, t)], \quad (22b)$$

where both the amplitude  $\mathcal{A}$  and phase  $\phi$  are changing very slowly. From Eqs. (22a) and (22b), we can easily find all the required spatial derivatives,

$$\begin{aligned} \zeta_{rr} = (2\mathcal{A}_r \phi_r + \phi_{rr} \mathcal{A}) \sin(\Omega t - \phi) \\ + (\mathcal{A}_{rr} - \mathcal{A} \phi_r^2) \cos(\Omega t - \phi), \end{aligned} \quad (23a)$$

$$\begin{aligned} u_{rr} = \Omega(\mathcal{A} \phi_r^2 - \mathcal{A}_{rr}) \sin(\Omega t - \phi) \\ + \Omega(2\mathcal{A}_r \phi_r + \phi_{rr} \mathcal{A}) \cos(\Omega t - \phi). \end{aligned} \quad (23b)$$

Further, with the aid of Eqs. (22a) and (22b), we acquire the following form of the amplitude dynamics:

$$\begin{aligned} \dot{\mathcal{A}} = -\frac{1}{\Omega}[\lambda h - \Omega^2(D_{22} + D_{12} + \frac{D_{12}}{\Omega^2} - D_{11} \\ - D_{21})\zeta_{rr} + (D_{22} + D_{11})u_{rr}] \sin(\Omega t - \phi), \end{aligned} \quad (24)$$

and the dynamical equation of phase,

$$\begin{aligned} \dot{\phi} = \frac{1}{\Omega \mathcal{A}} \left[ \lambda h - \Omega^2(D_{22} + D_{12} + \frac{D_{12}}{\Omega^2} - D_{11} \right. \\ \left. - D_{21})\zeta_{rr} + (D_{22} + D_{11})u_{rr} \right] \cos(\Omega t - \phi). \end{aligned} \quad (25)$$

Now by taking average over one cycle, fast oscillation parts can be easily ironed out and we obtain amplitude and phase equations of the Brusselator model in the presence of cross diffusion as

$$\begin{aligned} \dot{\mathcal{A}} = \mathcal{A} \lambda - p_1 \frac{3\lambda c_2 \Omega^2}{4} \mathcal{A}^3 + \frac{\Omega}{2} \left( D_{22} + D_{12} + \frac{D_{12}}{\Omega^2} - D_{11} - D_{21} \right) \\ \times (2\mathcal{A}_r \phi_r + \phi_{rr} \mathcal{A}) + \frac{(D_{11} + D_{22})}{2} (\mathcal{A}_{rr} - \mathcal{A} \phi_r^2), \end{aligned} \quad (26a)$$

$$\begin{aligned} \dot{\phi} = -p_2 \frac{\Omega}{8} \mathcal{A}^2 + \frac{(D_{11} + D_{22})}{2} \left( \frac{2\mathcal{A}_r \phi_r}{\mathcal{A}} + \phi_{rr} \right) \\ - \frac{\Omega}{2} \left( D_{22} + D_{12} + \frac{D_{12}}{\Omega^2} - D_{11} - D_{21} \right) \left( \frac{\mathcal{A}_{rr}}{\mathcal{A}} - \phi_r^2 \right). \end{aligned} \quad (26b)$$

To take into account the effect of non-negative term  $2\lambda c_1$  in Eq. (19) that generates unidirectional acceleration from unstable stationary point, correction factors,  $p_2$  and  $p_1$ , in phase shift and limit-cycle radius expression needs to be introduced [49].

### A. Hopf amplitude equation

The system dynamics near the onset of Hopf instability can be described by using the lowest-order amplitude equation as the CGLE [17,33,34]. From the phase and amplitude Eqs. (26b) and (26a) found by use of the KB method, we can arrive at a particular form which agrees with unscaled form of CGLE,

$$\frac{\partial Z}{\partial t} = \lambda Z + (\alpha_r + i\alpha_i) \partial_r^2 Z - (\beta_r - i\beta_i) |Z|^2 Z. \quad (27)$$

By setting  $Z = \mathcal{A} \exp(-i\phi)$  in Eq. (27) and separating real and imaginary parts one obtains

$$\frac{\partial \mathcal{A}}{\partial t} = \lambda \mathcal{A} - \beta_r \mathcal{A}^3 + \alpha_i (2\mathcal{A}_r \phi_r + \phi_{rr} \mathcal{A}) + \alpha_r (\mathcal{A}_{rr} - \mathcal{A} \phi_r^2), \quad (28a)$$

$$\frac{\partial \phi}{\partial t} = -\beta_i \mathcal{A}^2 + \alpha_r \left( \frac{2\mathcal{A}_r \phi_r}{\mathcal{A}} + \phi_{rr} \right) - \alpha_i \left( \frac{\mathcal{A}_{rr}}{\mathcal{A}} - \phi_r^2 \right). \quad (28b)$$

Equation (28a) and Eq. (28b) are exact deductions of the CGLE and represent amplitude and phase dynamics, respectively, near the onset of Hopf instability. Comparing Eqs. (28a) and (28b) with the dynamical equations of amplitude and phase derived by use of the KB method, Eqs. (26a) and (26b), we obtain these coefficients:  $\lambda = \frac{b-1-a^2}{2}$ ,  $\beta_r = p_1 \frac{3\lambda c_2 \Omega^2}{4}$ ,  $\beta_i = p_2 \frac{\Omega}{8}$ ,  $\alpha_r = \frac{(D_{11} + D_{22})}{2}$ ,  $\alpha_i = \frac{\Omega}{2} (D_{22} + D_{12} + \frac{D_{12}}{\Omega^2} - D_{11} - D_{21})$ . Now we will introduce the following scaled variables:

$$\mathcal{A} = \frac{\mathcal{A}}{\sqrt{\beta_r}}, \quad r = \frac{r}{\sqrt{\alpha_r}}.$$

This scaling will result in the following form of amplitude and phase equations:

$$\frac{\partial \mathcal{A}}{\partial t} = \lambda \mathcal{A} - \mathcal{A}^3 + \alpha (2\mathcal{A}_r \phi_r + \phi_{rr} \mathcal{A}) + (\mathcal{A}_{rr} - \mathcal{A} \phi_r^2), \quad (29a)$$

$$\frac{\partial \phi}{\partial t} = -\beta \mathcal{A}^2 + \left( \frac{2\mathcal{A}_r \phi_r}{\mathcal{A}} + \phi_{rr} \right) - \alpha \left( \frac{\mathcal{A}_{rr}}{\mathcal{A}} - \phi_r^2 \right), \quad (29b)$$

corresponding to normal form of complex Ginzburg-Landau equation [1,34,50] in one space dimension at the onset of Hopf instability in spatially extended system as

$$\frac{\partial Z}{\partial t} = \lambda Z + (1 + i\alpha) \partial_r^2 Z - (1 - i\beta) |Z|^2 Z. \quad (30)$$

Coefficients in normal form of CGLE are now solely the ratio between the imaginary and real parts of the complex coefficients of diffusive and nonlinear terms in Eq. (27) and are given by  $\alpha = \frac{\alpha_i}{\alpha_r} = \frac{\Omega(D_{22}+D_{12}+\frac{D_{12}^2}{\Omega^2}-D_{11}-D_{21})}{(D_{11}+D_{22})}$  and  $\beta = \frac{\beta_i}{\beta_r} = \frac{p_2}{p_1} \frac{1}{3a}$ . The coefficient  $\alpha$  found by using KB averaging in the case of the Brusselator model with cross diffusion exactly matches with the one found by using the rigorous method of the multiscale approach in Ref. [51]. It is quite apparent that the coefficient  $\alpha$  depends on the both self- and cross-diffusion terms explicitly in the case of Hopf instability. Another coefficient,  $\beta$ , does not have any dependence on diffusion and is given in Ref. [17] as  $\beta = \frac{4-7a^2+4a^4}{3a(2+a^2)}$  for the Brusselator model. Properties of uniform oscillations can be obtained from Eq. (30) by considering a simple and general state of nonlinear oscillations as

$$Z = \mathcal{A} \exp(i\omega_0 t), \quad (31)$$

where  $\omega_0$  is the shift in frequency from the critical frequency  $\omega_{cH}$  [1]. Now by inserting it into normal CGLE (30) and comparing imaginary and real parts, we get  $\mathcal{A}^2 = \lambda$  and  $\omega_0 = \beta \mathcal{A}^2 = \beta \lambda$ . As  $\beta$  is a nonlinear phase shift, it captures dependence of oscillation frequency on the magnitude of the amplitude and wave-number shift. Hence nonlinear oscillations for Hopf bifurcation can be specified from Eq. (31) as

$$\mathcal{A}_H = \sqrt{\lambda} \exp(i\beta \lambda t). \quad (32)$$

### B. Turing amplitude

The amplitude equation corresponding to Turing instability is known as the Turing amplitude equation (TAE) which is the real counterpart of the CGLE. Near the onset of Turing instability, the lowest-order case of one-dimensional TAE can simply be constructed by the symmetry argument [1] as

$$\frac{\partial Z}{\partial t} = \lambda_T Z + \varrho \partial_r^2 Z - g |Z|^2 Z, \quad (33)$$

where  $\lambda_T = \frac{b-b_c}{2}$  is defined in similar way as  $\lambda$  in Hopf instability and  $\varrho$  and  $g$  are coefficients containing details of the system. By setting  $Z = \mathcal{A} \exp(-i\phi)$  in Eq. (33) and then separating the real and imaginary parts we obtain

$$\frac{\partial \mathcal{A}}{\partial t} = \lambda_T \mathcal{A} - g \mathcal{A}^3 + \varrho (\mathcal{A}_{rr} - \mathcal{A} \phi_r^2), \quad (34a)$$

$$\frac{\partial \phi}{\partial t} = \varrho \left( \frac{2\mathcal{A}_r \phi_r}{\mathcal{A}} + \phi_{rr} \right). \quad (34b)$$

We are only interested in bifurcation scenario of generic dynamical features of the system here and hence it is enough to have only parameter  $\lambda_T$  in TAE. Now, by introducing the following scales in amplitude and spatial dimension,

$$\mathcal{A} = \frac{A}{\sqrt{g}}, r = \frac{r}{\sqrt{\varrho}}$$

and taking constant phase value by virtue of translational invariance of spatial pattern in Eqs. (34a) and (34b) we find

$$\frac{\partial \mathcal{A}}{\partial t} = \lambda_T \mathcal{A} - \mathcal{A}^3 + \mathcal{A}_{rr}, \quad (35a)$$

$$\frac{\partial \phi}{\partial t} = 0, \quad (35b)$$

where  $b_{cT}$  in  $\lambda_T = \frac{b-b_{cT}}{2}$  is given by the Eq. (13) and it contains all the effect of self-diffusion as well as cross-diffusion constant. Equations (35a) and (35b) are deduction of normalized form of TAE for the case of constant phase as

$$\frac{\partial Z}{\partial t} = \lambda_T Z + \partial_r^2 Z - |Z|^2 Z, \quad (36)$$

which could be simply regarded as special case of the normal form of CGLE (30) if  $\alpha$  and  $\beta$  are set to zero [33]. Equation (35a) admits a time-dependent homogeneous solution of Turing amplitude as

$$\mathcal{A}_T^2 = \mathcal{A}_s^2 \left\{ \frac{1}{1 - \mathcal{A}_0 \exp[-2\lambda_T(t - t_0)]} \right\}, \quad (37)$$

which renders  $\mathcal{A}_T = \sqrt{\lambda_T}$  for the long-time limit.

### V. ENTROPY PRODUCTION RATE

For a chemical reaction network, fluxes are not a linear function of the conjugate force. Net reaction currents of reversible chemical reactions are given as the difference between forward and reverse fluxes of reactions:

$$j_\rho = j_{+\rho} - j_{-\rho}, \quad (38)$$

where  $+$  and  $-$  label forward reaction and backward reaction, respectively. Since  $k_{-\rho} \simeq 0$  is assumed in Sec. II, all the reverse reaction fluxes are negligibly small, i.e.,  $j_{-\rho} \simeq 0$ . Concentration fluxes according to the law of mass action are

$$j_{\pm\rho} = k_{\pm\rho} \prod_{\sigma} z_{\sigma}^{v_{\pm\rho}^{\sigma}}, \quad (39)$$

where  $v_{\pm\rho}^{\sigma}$  denotes the number of molecules of a particular species  $\sigma$  for forward ( $+$ ) or reverse ( $-$ ) direction of reaction  $\rho$ . Whereas, according to Fick's diffusion law, the diffusion current is proportional to the gradient of the concentration distribution of diffusing species and in a one-dimensional system simply reduces to

$$J_{\sigma} = -D \frac{\partial z_{\sigma}}{\partial r}, \quad (40)$$

with constant diffusion coefficient  $D$  being one of the the elements of the matrix  $\mathcal{D} = \begin{pmatrix} D_{11} & D_{12} \\ D_{21} & D_{22} \end{pmatrix}$  in the presence of the cross diffusion.

The product of the stoichiometric coefficient of species  $\sigma$  of a particular reaction step  $\rho$  and corresponding chemical potential  $\mu_{\sigma}$  gives the thermodynamic driving forces of reaction known as reaction affinities [52]:

$$f_{\rho} = - \sum_{\sigma} S_{\rho}^{\sigma} \mu_{\sigma}, \quad (41)$$

where  $S_\rho^\sigma = v_{-\rho}^\sigma - v_{+\rho}^\sigma$  and  $\mu_\sigma = \mu_\sigma^o + \ln \frac{z_\sigma}{z_0}$  with solvent concentration  $z_0$  and standard-state chemical potential  $\mu_\sigma^o$ . To define a baseline for substances, standard-state quantities with notation  $o$  are defined at standard pressure  $p = p^o$  and molecular concentration and chemical potential and  $\mu_\sigma$  characterizes each chemical species of the dilute solution thermodynamically. The system is maintained at constant absolute temperature  $T$  fixed by the solvent, and, for simplicity,  $RT$  is taken as unity. Using this form of the chemical potential local detailed balance condition of the the reaction steps can be expressed as:

$$\ln \frac{k_{+\rho}}{k_{-\rho}} = - \sum_{\sigma} S_\rho^\sigma \mu_\sigma^o. \quad (42)$$

Hence reaction affinities in Eq. (41) can be written in terms of the reaction fluxes of the chemical steps as

$$f_\rho = \ln \frac{j_{+\rho}}{j_{-\rho}}. \quad (43)$$

Equation (42) is very important one as it relates the dynamical term with thermodynamic entity. Similarly to reaction affinity, a thermodynamic driving force, local diffusion affinity, exists in the reaction-diffusion system and can be expressed as a gradient of the chemical potential,

$$F_\sigma = - \frac{\partial \mu_\sigma}{\partial r}. \quad (44)$$

Entropy production rate (EPR) due to the chemical reaction can be expressed as the product of the thermodynamic driving force and reaction flux as

$$\frac{d\Sigma_R}{dt} = \frac{1}{T} \int dr \sum_{\rho} f_\rho j_\rho. \quad (45)$$

So with the help of the Eq. (43) and Eq. (38), we obtain EPR due to reaction as

$$\frac{d\Sigma_R}{dt} = \frac{1}{T} \int dr \sum_{\rho} (j_{+\rho} - j_{-\rho}) \ln \frac{j_{+\rho}}{j_{-\rho}}, \quad (46)$$

considering the elementary reaction steps which are directly related to reaction stoichiometry.

Similarly, entropy production rate due to diffusion can be simply

$$\frac{d\Sigma_D}{dt} = \frac{1}{T} \int dr \sum_{\sigma} F_\sigma J_\sigma. \quad (47)$$

Considering diffusive flux and affinity given in the Eqs. (40) and (44), respectively, we have

$$\begin{aligned} \frac{d\Sigma_D}{dt} = \int dr \left[ D_{11} \left\| \frac{\partial x}{\partial r} \right\|^2 + D_{22} \left\| \frac{\partial y}{\partial r} \right\|^2 \right. \\ \left. + D_{12} \frac{\left\| \frac{\partial y}{\partial r} \right\| \left\| \frac{\partial x}{\partial r} \right\|}{x} + D_{21} \frac{\left\| \frac{\partial x}{\partial r} \right\| \left\| \frac{\partial y}{\partial r} \right\|}{y} \right]. \quad (48) \end{aligned}$$

The last two terms on the right-hand side in Eq. (48) correspond to the cross-diffusion coefficients of the intermediate species present in the system.

Total entropy production is simply the sum of reaction EPR and diffusion EPR,

$$\dot{\Sigma} = \dot{\Sigma}_R + \dot{\Sigma}_D \geq 0. \quad (49)$$

In contrast, a closed system must relax to the thermodynamic equilibrium, and as a consequence the concentration distribution of the species will be distributed homogeneously over the system. At thermodynamic equilibrium all the internal fluxes, i.e.,  $j_\rho$  and  $J_\sigma$ , and external fluxes of the chemostatted species vanish and so the total entropy production rate is zero.

## VI. NONEQUILIBRIUM GIBBS FREE ENERGY OF CHEMOSTATIC SYSTEM

Nonequilibrium Gibbs free energy of a chemical reaction network can be expressed in terms of the Gibbs free energy of an ideal dilute solution ([53], ch. 7) as

$$G = G_0 + \int dr \sum_{\sigma \neq 0} (z_\sigma \mu_\sigma - z_\sigma), \quad (50)$$

where  $G_0 = z_0 \mu_0^o$ . A constant term like  $\ln z_0$  is also absorbed within  $\mu_\sigma^o$  term of chemical potential. Here the solvent has been treated as a special chemostatted element and both  $G^0$  and  $\sum_{\sigma \neq 0} z_\sigma$  in Eq. (50) are due to solvent of dilute solution. For a closed system, when the concentration distribution is relaxed to a unique equilibrium distribution,  $z_\sigma^{\text{eq}}$ , from Eq. (50) one finds

$$G(z_\sigma^{\text{eq}}) = G_0 + \int dr \sum_{\sigma \neq 0} (z_\sigma^{\text{eq}} \mu_\sigma^{\text{eq}} - z_\sigma^{\text{eq}}). \quad (51)$$

The left null vectors corresponding to the left null space of the stoichiometric matrix are known as the conservation laws ([32], pp. 89–103), whereas the (right) null eigenvectors of the stoichiometric matrix represent cycles. So, mathematically, conservation law can be expressed as

$$\sum_{\sigma} l_\sigma^\lambda S_\rho^\sigma = 0, \quad (52)$$

where

$$S_\rho^\sigma \in \mathbb{R}^{\sigma \times \rho}, \{l_\sigma^\lambda\} \in \mathbb{R}^{(\sigma-w) \times \sigma}, w = \text{rank}(S_\rho^\sigma).$$

From the definition of affinity in Eq. (41), we can further express chemical potentials in terms of linear combination of conservation laws for a closed system at equilibrium,

$$\mu_\sigma^{\text{eq}} = R_\lambda l_\sigma^\lambda, \quad (53)$$

where  $R_\lambda$  is real coefficient with dimension of force. Conserved quantities of a closed system known as components can be specified in terms of this conservation laws of the reaction network with

$$L_\lambda = \sum_{\sigma} l_\sigma^\lambda z_\sigma, \quad (54)$$

such that  $\frac{d}{dt} \int dr L_\lambda = 0$ . Since components  $L_\lambda$  remain constant over time for a closed reaction-diffusion system, it would characterize both the equilibrium and nonequilibrium concentration distributions as  $\mu_\sigma^{\text{eq}} z_\sigma^{\text{eq}} = \mu_\sigma^{\text{eq}} z_\sigma$ . This renders

another form of Eq. (51) as

$$G(z_\sigma^{\text{eq}}) = G_0 + \int dr \sum_{\sigma \neq 0} (z_\sigma \mu_\sigma^{\text{eq}} - z_\sigma^{\text{eq}}). \quad (55)$$

Using the relation in Eq. (53) we could also have the following expression of equilibrium Gibbs free energy from Eq. (51):

$$G^{\text{eq}} = G(z_\sigma^{\text{eq}}) = G_0 + \int dr \sum_{\sigma \neq 0} (R_\lambda L_\lambda - z_\sigma^{\text{eq}}). \quad (56)$$

In the information theory approach [54], Shannon entropy or Kullback-Leibler divergence is defined for two normalized probability distributions,  $P$  and  $P^0$ , as

$$\Gamma(P||P^0) = \sum_i P_i \log \frac{P_i}{P_i^0}$$

and it quantifies the amount of information needed to switch from a known distribution  $P^0$  to the distribution  $P$ . With the similar spirit, we can express nonequilibrium Gibbs free energy by exploiting Eqs. (50) and (55) as

$$G - G^{\text{eq}} = \Gamma(z_\sigma || z_\sigma^{\text{eq}}), \quad (57)$$

where

$$\Gamma(z_\sigma || z_\sigma^{\text{eq}}) = \sum_\sigma \left\{ z_\sigma \log \frac{z_\sigma}{z_\sigma^{\text{eq}}} - (z_\sigma - z_\sigma^{\text{eq}}) \right\} \geq 0$$

is relative entropy for non-normalized concentration distribution. Thus Eq. (57) implies that the lowest possible value of the nonequilibrium Gibbs free energy is set by its equilibrium counterpart in a closed system.

Conservation laws in an open system could be characterized in general by

$$l_T^\lambda S_\rho^I + l_C^\lambda S_\rho^C = 0 \begin{cases} l_T^{\lambda_b} S_\rho^I \neq 0 & \text{broken CL} \\ l_T^{\lambda_u} S_\rho^I = 0 & \text{unbroken CL} \end{cases}, \quad (58)$$

where for an open system,  $\{\lambda\} = \{\lambda_b\} \cup \{\lambda_u\}$ , labels  $u$  and  $b$  correspond to unbroken and broken ones, respectively. So from Eq. (58), we can say broken conservation laws are not left null vectors of  $S_\rho^I$  for at least one reaction of the reaction network. Consequently, corresponding broken components,  $L_{\lambda_b}$ , of open system are no longer a global conserved quantities. Depending on whether chemostatted species break a conservation law or not, a set of chemostatted species could thus be divided into two subsets so that  $\{C\} = \{C_b\} \cup \{C_u\}$ .

The semigrand Gibbs free energy of the open system can be acquired from the nonequilibrium Gibbs free energy as

$$\mathcal{G} = G - \sum_{C_b} \mu_{C_b}^{\text{eq}} M_{C_b}, \quad (59)$$

where  $M_{C_b} = \sum_{C_b} l_{C_b}^{\lambda_b^{-1}} \int dr L_{\lambda_b}$  resembles moieties that are exchanged between chemostats and a system only through the external flow of the chemostatted species. For an open system, nonequilibrium semigrand Gibbs free energy will have a form similar to its nonequilibrium Gibbs free-energy counterpart,

$$\mathcal{G} = \mathcal{G}^{\text{eq}} + \Gamma(z_\sigma || z_\sigma^{\text{eq}}). \quad (60)$$

At the local level, exchange of species between neighboring spaces due to local diffusion will be equivalent to matter exchange through chemostatting. So the energetic contribution

of the species exchanged through the local diffusion needs to be eliminated to define proper thermodynamic potential at the local level of the open reaction-diffusion system [36]. So from the local standpoint, the transformed Gibbs free energy would have the following form:

$$\mathcal{G}_{\mathcal{L}} = G - \mu_\sigma^{\text{eq}} z_\sigma, \quad (61)$$

where  $G$  is the Gibbs free energy of the system is specified at each point of the system. When all the conservation laws are broken then  $\mu_I^{\text{eq}} z_\sigma = \mu_{C_b}^{\text{eq}} l_{C_b}^{\lambda_b^{-1}} l_I^{\lambda_b} z^I$  and  $\mu_{C_b}^{\text{eq}} z_\sigma = \mu_{C_b}^{\text{eq}} l_{C_b}^{\lambda_b^{-1}} l_{C_b}^{\lambda_b} z^{C_b}$  and thus Eq. (61) would result in expression identical to Eq. (59).

For the stoichiometric matrix (2) of the Brusselator reaction network, the conservation laws of the closed reaction-diffusion system are represented by two linearly independent ( $1 \times 6$ ) vectors,

$$l_\sigma^{\lambda=1} = \begin{pmatrix} X & Y & A & B & D & E \\ 1 & 1 & 1 & 0 & 0 & 1 \end{pmatrix} \quad (62)$$

and

$$l_\sigma^{\lambda=2} = \begin{pmatrix} X & Y & A & B & D & E \\ 0 & 0 & 0 & 1 & 1 & 0 \end{pmatrix}. \quad (63)$$

The components corresponding to these two conservation laws are  $L_1 = x + y + a + e$  and  $L_2 = b + d$ . The species  $A$  and  $B$  are considered as the reference chemostatted species here and both the conservation laws of the Brusselator model in Eqs. (62) and (63) are broken by chemostatting of  $A$  and  $B$ .

## VII. CONCENTRATION FIELDS OF INTERMEDIATE SPECIES

As mentioned earlier in Sec. III B, we can have both Turing and Hopf instabilities in reaction-diffusion system. The spatiotemporal profile of the concentration fields in a different range of control parameters shows periodic behavior depending on the dispositions of the Turing and Hopf instabilities. The resulting pattern can be traced in the critical wave numbers and frequencies of Turing and Hopf regimes from the solution of the corresponding amplitude equations.

### A. Turing instability regime

For the marginal stability condition of the homogeneous state of the system, the growth rate becomes zero and the evolution equation of the concentration field near the onset of Turing instability can be expressed by using an amplitude equation formalism for the single fastest-growing mode as

$$z_{IT} = z_{I0} + A_T U_{cT} \exp(iq_{cT} r) + \text{c.c.}, \quad (64)$$

where  $Z_{I0} \in [x_0, y_0]$  is a time-independent uniform base state with respect to extended direction and  $A_T$  is a Turing amplitude rendering several essential features of the pattern formation. The corresponding long-time solution of Eq. (64) is given by

$$\begin{pmatrix} x \\ y \end{pmatrix} = \begin{pmatrix} x_0 \\ y_0 \end{pmatrix} + \left\{ \left[ \frac{1}{-\frac{k_4}{k_1} \sqrt{\frac{k_4}{k_3} \frac{\sqrt{\det(D)}}{(D_{12}+D_{22})a}} - \frac{(D_{21}+D_{11})}{(D_{12}+D_{22})}} \right] \times A_T 2 \cos q_{cT} r \right\}. \quad (65)$$



### B. Hopf instability regime

Similarly to the Turing instability in Sec. VII A, the perturbation part in the Hopf instability can be written as

$$\delta z_I = A_H U_{cH} \exp(i\omega_{cH}t) + \text{c.c.}, \quad (66)$$

where  $A_H$  is the Hopf amplitude part. The final equation of the perturbation can be expressed as

$$\begin{pmatrix} \delta x \\ \delta y \end{pmatrix} = \sqrt{\lambda} \exp(i\beta\lambda t) \left\{ \begin{array}{l} 2 \cos(\omega_{cH}t + \beta\lambda t) - \frac{2}{a} \sqrt{\frac{k_4}{k_3}} \frac{1}{k_1} \sin(\omega_{cH}t + \beta\lambda t) \\ -2(1 + \frac{k_4^3}{k_3 k_1^2} \frac{1}{a^2} \cos[\omega_{cH}t + \beta\lambda t]) \end{array} \right\}. \quad (67)$$

For the parameter value greater than the critical value  $b_{cH}$ , this perturbation part will give rise to the limit-cycle type oscillatory profile.

### C. Overlapping of Turing and Hopf instabilities

Here we are going beyond the Turing condition of pattern formation and we have chosen equal self-diffusion coefficients and nonzero cross-diffusion coefficients for the Brusselator model. Critical values of the control parameter  $b$  for Turing and Hopf instabilities are given previously by Eq. (13) in Sec. III and (16) in Sec. III B, respectively. Equating these, we can simply derive a particular point  $a_{TH}$  in the parameter space of  $a$  for which thresholds of Turing and Hopf instabilities would coincide in the  $(a, b)$  parameter plane as

$$a_{TH} = \left[ \frac{k_4^3}{k_3 k_1^2} \right]^{\frac{1}{2}} \left( \frac{[\det(\mathcal{D})]^{\frac{1}{2}} + \sqrt{[\det(\mathcal{D})] - [D_{22} + D_{12} - D_{11} - D_{21}]D_{12}}}{[D_{22} + D_{12} - D_{11} - D_{21}]} \right). \quad (68)$$

In the vicinity of the Turing-Hopf point, the critical intrinsic wave number of the Turing instability obtained from the marginal stability condition is given by

$$q_{cT}|_{a=a_{TH}} = q_{cTH} = \left[ \frac{k_1^2 k_3}{k_4} \frac{a_{TH}^2}{\det(\mathcal{D})} \right]^{\frac{1}{4}}$$

and the critical frequency of a homogeneous Hopf mode is  $\omega_{cTH} = a_{TH}$ . Superposition of the Turing mode in Eq. (64) and the Hopf mode in Eq. (66) will describe the spatiotemporal dynamics of the concentration field due to Turing-Hopf interplay with

$$z_{ITH} = z_{I0} + A_T U_{cT} \exp(iq_{cT}r) + A_H U_{cH} \exp(i\omega_{cH}t) + \text{c.c.} \quad (69)$$

This concentration field is employed to assess all the thermodynamic entities corresponding to Turing-Hopf interplay.

We have considered spatiotemporal pattern arising from the interplay between Turing and Hopf instabilities in either of following three ways:

- (i) The stationary spatial Turing pattern grows before it loses stability as control parameter  $b$  is further changed and Hopf instability appears in the reaction-diffusion system.
- (ii) Homogeneous oscillatory pattern emerges first and then the limit-cycle solution modulated by Turing instability emerges.
- (iii) Critical points of Turing and Hopf instabilities overlap and thus they arise simultaneously in the system and interact.

Based on the amplitude equation formalism in the presence of cross diffusion, we obtain concentration profiles for all three scenarios with the aid of Eq. (68) in the space of control parameter  $b$ , which lies in the vicinity of onset of instabilities.

## VIII. RESULTS AND DISCUSSIONS

The evolution of the entropy production rate and semigrand Gibbs free energy in the 1D Brusselator model regarded as an open chemical network has been investigated analytically to find out the correspondence between the evolution of thermodynamic quantities and spatiotemporal pattern due to Turing-Hopf interplay. All the results correspond to a steady-state condition with absolute temperature  $T = 300$  K; diffusion coefficients  $D_{11} = D_{22} = 1, D_{12} = 0.51, D_{21} = -0.51$ , one-dimensional system length  $l = 9.5$ ; and for the weakly reversible case, i.e., chemical reaction rate constants  $k_{-\rho} = 10^{-4} \ll k_{\rho} = 1$ , unless otherwise indicated. The temperature is constant throughout the system as the rate of heat diffusion is assumed to be much faster than the diffusion rate of species. We have used  $b$  as control parameter to find its effect on the intermediate species concentrations and thus on the thermodynamic entities also.

In Fig. 2(a), we show the region of Turing-Hopf interplay in  $(b, a)$  parameter space. We have obtained the Turing line by using Eq. (13) and the Hopf line by using Eq. (16) as shown by a solid line and a dashed line, respectively. The circular label in the figure corresponds to the critical Turing-Hopf point where the Turing and Hopf lines intersect.

Exploiting the modified Taylor dispersion method, the values of the self-diffusion, as well as cross-diffusion, coefficients are experimentally determined in the case of three-component [55], four-component [55,56], and five-component [57] Belousov-Zhabotinsky reaction dispersed in Aerosol OT water-in-oil microemulsion (BZAOT) systems [58,59]. In their work, Rossi *et al.* reported that experimentally found cross-diffusion coefficients can shift the Turing onset and thus can generate a Turing pattern if the system was initially close to the onset of instability. To obtain proper insight of this experimental claim, we have also taken diffusion matrix

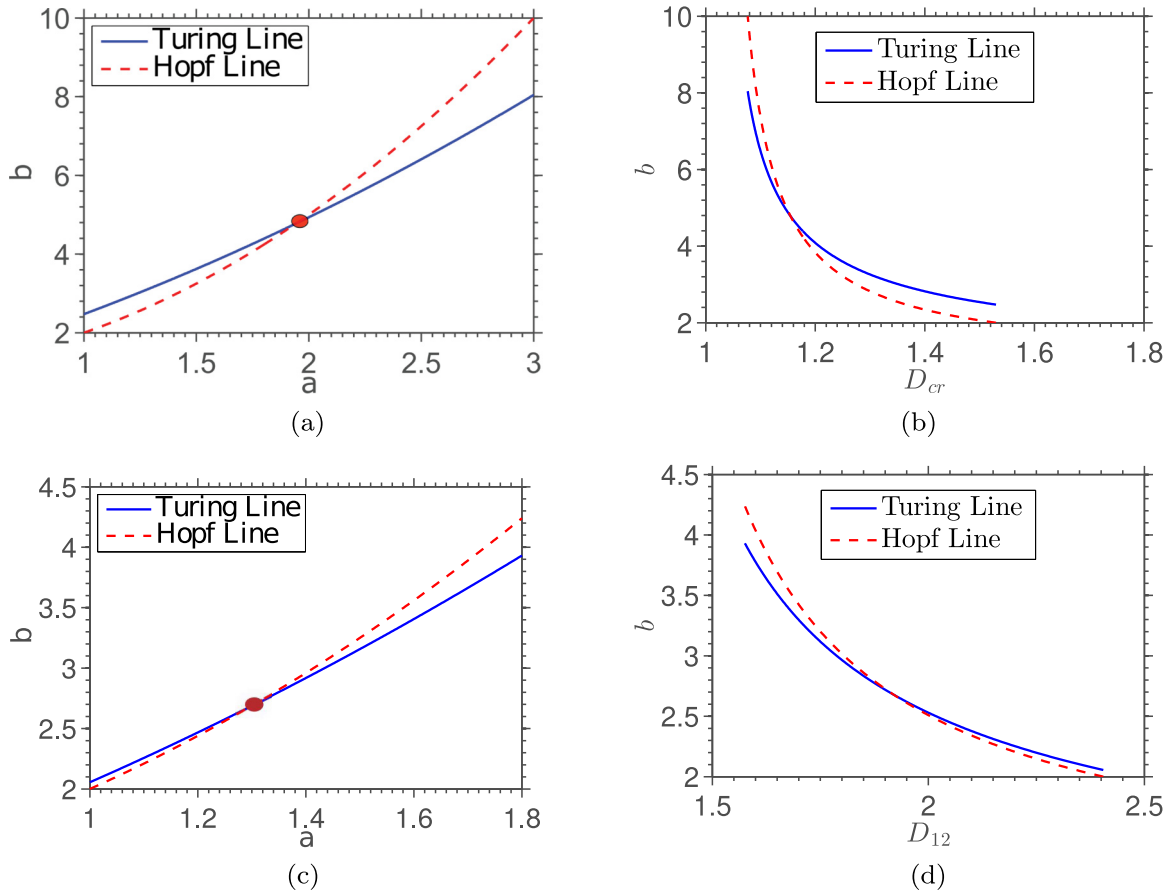


FIG. 2. The solid line is the Turing line corresponding to Eq. (13) and the dashed curve is the Hopf line corresponding to Eq. (16) in both (a) and (b) in the presence of the diffusion coefficients  $D_{11} = D_{22} = 1$ ,  $D_{12} = 0.51$ , and  $D_{21} = -0.51$ . In panel (a), the point of intersection of the Turing and Hopf lines is  $[a_{TH} \approx 1.9438, b_{cT} = b_{cH} \approx 4.7785]$ . In (b), we have defined a new parameter,  $D_{cr} = D_{12}[1 + \frac{1}{a^2}] - D_{21}$ , containing only cross-diffusion coefficients to explore the effect of cross diffusion on the Turing and Hopf lines. Panels (c) and (d) are similar to the previous figures with experimental magnitudes of the diffusion coefficients as  $D_{11} = 1.28$ ,  $D_{12} = 1.26$ ,  $D_{21} = -0.005$ , and  $D_{22} = 1.51$  of the pentanary BZ-AOT system.

elements from the experimental data of a pentanary BZAOT system [57] as  $D_{11} = 1.28$ ,  $D_{12} = 1.26$ ,  $D_{21} = -0.005$ , and  $D_{22} = 1.51$  on the ground of the assumption that the presence of additional components in the system leaves the diffusion coefficients unchanged [56] and the corresponding results are shown in Figs. 2(c) and 2(d). One should note that the effect of cross diffusion on the onset of Turing instability for the BZ-AOT system was reported in the presence of two different self-diffusion coefficients. Although, from Fig. 2(b), it is clear that  $D_{cr}$  composed of cross-diffusion coefficients can control the onset of instabilities even when all the self-diffusion coefficients are equal [51].

When cross diffusion has a linear dependence on the concentration, we can write the cross-diffusion coefficients as  $D_{12} = D_{12}x_0$  and  $D_{21} = D_{21}y_0$  [19,20] with  $x_0 = \frac{k_1}{k_4}a$  and  $y_0 = \frac{k_2k_4b}{k_1k_3a}$  being the steady-state concentrations of  $X$  and  $Y$ , respectively, for the spatially homogeneous system. As  $A$  and  $B$  are chemostatted species and kinetic rate constants are fixed at a particular value throughout the time of interest,  $D_{21}$  and  $D_{12}$  are effectively constant in this case also. From Fig. 3(a), it is clear that the intersection of the Turing and Hopf lines is shifted to lower values of  $a$  and  $b$  due to this concentra-

tion dependence. In this context by taking only one nonzero cross-diffusion coefficient at a time, we have shown the effect of individual cross-diffusion coefficients on the Turing-Hopf intersection in Fig. 3(c) and Fig. 3(d) for equal self-diffusion coefficients. From Figs. 3(a) and 3(d), it is evident that modification of the Turing line due to concentration-dependent  $D_{21}$  is comparable to the effect of concentration  $a$  on the Turing line. From Figs. 3(b), 3(c), and 3(d), one can conclude that  $D_{21}$  has a stronger effect on the Turing line in the case of the Brusselator model. The more general concentration dependence of cross-diffusion terms is beyond the scope here.

We now consider three different values of  $a$  for three different scenarios, i.e.,  $a = 2.1$  (Turing instability precedes Hopf instability),  $a \approx 1.9438$  Codimension 2 (COD2), and  $a = 1.8$  (Hopf instability arises first) in subsequent studies. In Fig. 2(b), we explore the Turing and Hopf lines as a function of the newly defined parameter,  $D_{cr} = D_{12}[1 + \frac{1}{a^2}] - D_{21}$ , motivated by the fact that cross-diffusion coefficients are present explicitly in this part and  $D_{cr}$  appears in both Eqs. (26a) and (26b) of amplitude and phase dynamics.

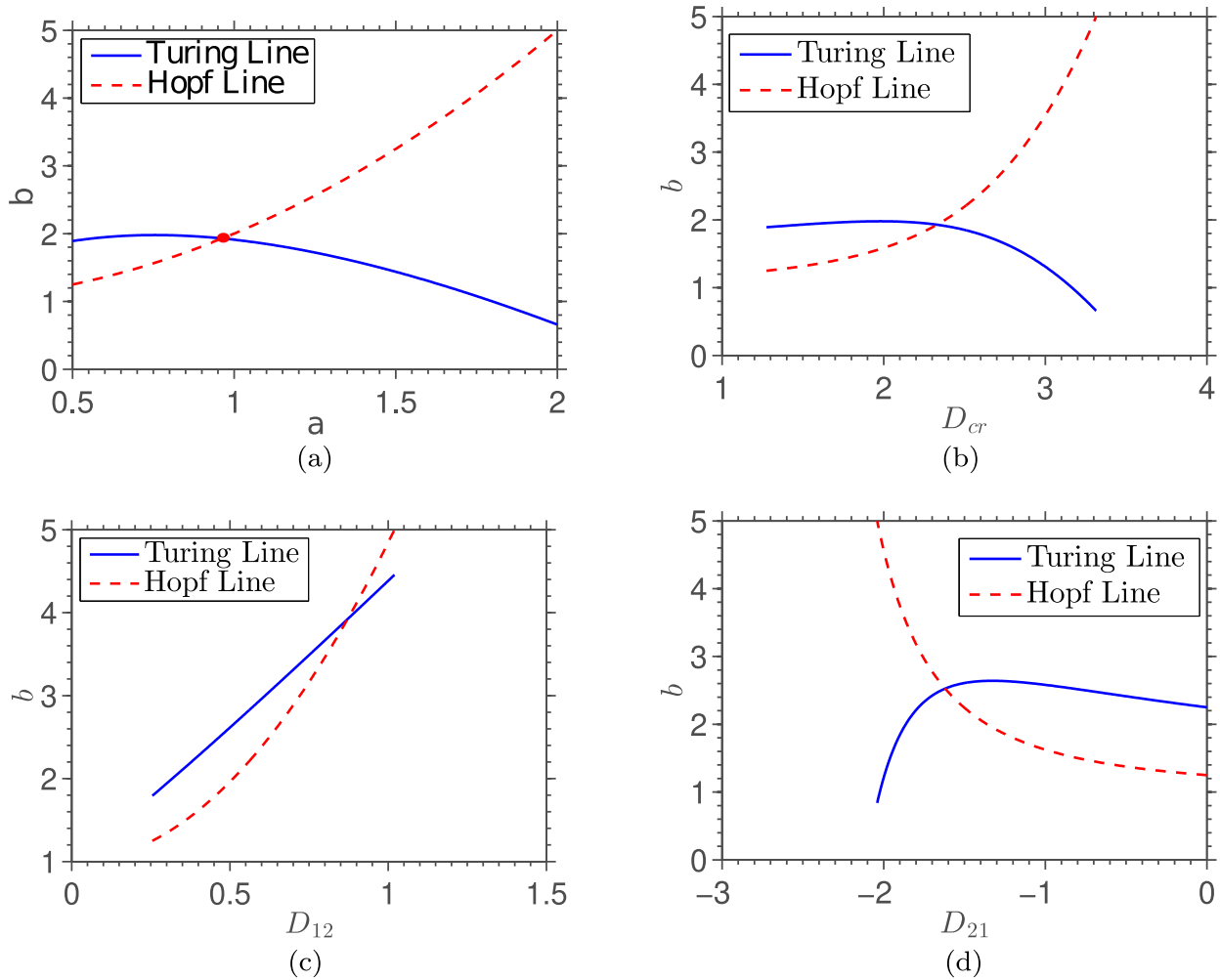


FIG. 3. The solid line is the Turing line, and the dashed curve is the Hopf line in both (a) and (b) in the presence of following diffusion coefficients:  $D_{11} = D_{22} = 1$ ,  $D_{12} = 0.51x_0$ , and  $D_{21} = -0.51y_0$ . In (a), the point of intersection of Turing and Hopf line is shifted to lower values of  $a$  and  $b$  due to concentration-dependent cross-diffusion coefficients. In (b), the parameter,  $D_{cr} = D_{12}[1 + \frac{1}{a^2}] - D_{21}$ , contains only cross-diffusion coefficients show the effect of concentration-dependent cross-diffusion coefficients on the Turing and Hopf lines. Panels (c) and (d) represent the individual effect of the cross-diffusion coefficients  $D_{12}$  and  $D_{21}$ , respectively.

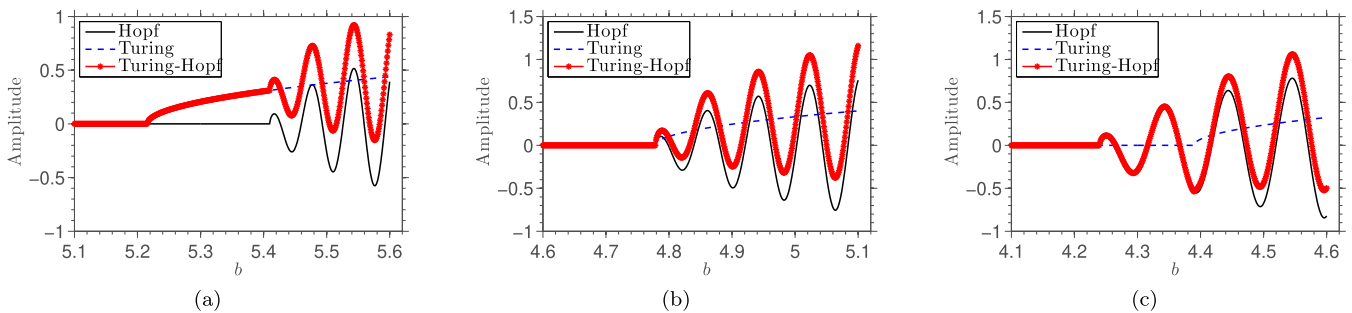


FIG. 4. The solid black line corresponds to the Hopf amplitude derived analytically as a function of control parameter  $b$  of the system at time  $t = 150$ . The blue dashed line refers to the Turing amplitude obtained from the analytical amplitude equation of the Turing instability. The red line plot with marker  $*$  shows addition of Turing and Hopf amplitudes. Three different scenarios of Turing-Hopf interplay have been shown here: (a) for  $a = 2.1$ , Turing first; (b) for COD2-Turing and Hopf appear simultaneously at the same point in parameter space; (c) for  $a = 1.8$ , Hopf first. Here we have analyzed all three cases at a particular local point of the finite system of length  $l = 9.5$ . This figures of amplitude will give lucid idea about local concentration profile in 1D Brusselator model in the parameter space of Turing-Hopf interplay and the effect of Hopf instability on the diffusion-driven Turing instability.

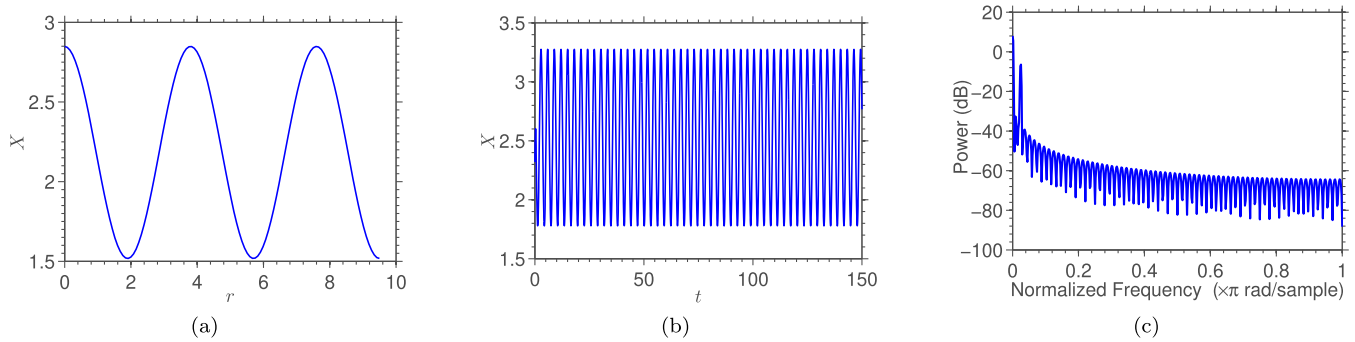


FIG. 5. Spatial and temporal dynamics of concentration  $X$  for the scenario when the Turing and Hopf modes arise simultaneously in a 1D Brusselator model with a system size of  $l = 9.5$ . Here  $a = a_{\text{TH}}$  and  $b = 4.9998$  and both self- and cross diffusion are present. The spatial pattern in (a) corresponds to a fixed time  $t = 150$ . Whereas the temporal pattern in (b) corresponds to a particular point of the system. Existence of these two structures is due to Turing instability and Hopf instability, respectively. Panel (c) shows the power spectral density estimate of discrete-time concentration vector of species  $X$  [see panel (b)] obtained via Welch's method.

In Fig. 4, we have shown the amplitude dynamics of Hopf and Turing with the aid of Eqs. (32) and (37). As the control parameter  $b$  is changed through the critical values of Turing and Hopf instabilities, we can see how the oscillatory behavior of Hopf instability dominates over diffusion-driven Turing instability for steady state at a given point of the system at time  $t = 150$ . Conversely, these figures also depict how the Turing instability modifies the oscillatory amplitude. As a consequence of this modification in oscillatory profile, the radius of the corresponding limit cycle will also change. In another way, it shows the effect of diffusion on the Hopf limit cycle indirectly through Turing instability. This amplitude profile renders clear the idea about local concentration profile in the parameter space of the Turing-Hopf interplay. Above all, these figures are the measure of both Turing and Hopf instabilities at fundamental level.

In Fig. 5, the spatial and temporal profiles of the concentration for a given value of the control parameter show periodic behavior due to Turing and Hopf instability, respectively. The spatial profile in Fig. 5(a) corresponds to a wave number close to the critical value of the Turing intrinsic critical wave number. Whereas the temporal oscillation in Fig. 5(b) has nonzero normalized frequency as seen by the peak in the power spectral density in Fig. 5(c). For the profiles in Fig. 5, we have considered only the scenario when the Turing and Hopf instabilities arise simultaneously at a point in parameter space. For other two scenarios these profiles have roughly the same features.

We have studied the response of the total entropy production rate due to the changes in reference chemostatted species,  $b$ , while another reference chemostatted species,  $a$ , remains constant. A nonzero total entropy production rate changes continuously and shows that an oscillatory response for all three scenarios (as mentioned above) arises in Turing-Hopf interplay as shown in Figs. 6(a), 6(c), and 6(e). Comparison among profiles of global concentration of activator (or inhibitor) in the right column of Fig. 6 and the corresponding total EPR on the left column of the same figure reveals that the total entropy production rate is quantitatively proportional to the total concentration of activator (or inhibitor) in the reaction-diffusion system. Moreover, they are showing qualitatively similar dynamics for all three cases. In other

words, the entropy production rate reflects the global dynamics of reaction-diffusion system concentration arising from the Turing-Hopf interplay. This result simply implies that the entropy production rate of a dissipative system can measure the pattern formation quantitatively as well as qualitatively.

Analytical concentration field of an intermediate species,  $X$ , as a function of control parameter  $b$  due to the Turing-Hopf interplay as shown in the first two rows of Fig. 7 is calculated by using Eq. (69) in Sec. VII C. The corresponding reaction and diffusion entropy production rate is obtained from Eqs. (46) and (48), respectively, in the presence of cross diffusion. The study of entropy production rate separately for diffusion and reaction reveals their proper contribution to total entropy production. It also renders clearly how Turing-Hopf interplay and cross diffusion modify these two parts separately. In Fig. 7(g), as the parameter value reaches the Turing instability critical point, the nonzero entropy production rate due to both reaction and diffusion shows initially dynamical bifurcation types of characteristics. Then the appearance of Hopf instability modifies the reaction part of the entropy production rate by its innate limit-cycle-type oscillatory dynamics and gives rise to irregular oscillatory response of the entropy production rate with respect to parameter  $b$ . The dotted red line in the same figure also shows modification of the diffusive entropy production rate by Hopf instability to a very little but finite extent and thus hints that the limit cycle of the Hopf instability has indirect dependence on the diffusion. In Fig. 7(i), initially Hopf instability is only present in the reaction-diffusion system and the entropy production rate is zero. Then as the control parameter changes and exceeds the Turing critical point, a nonzero diffusion entropy production rate appears due to Turing instability. This means that the thermodynamic entity is modified by the Turing instability in this framework although Hopf instability appears first. It is an interesting result, as in the dynamical framework, Hopf instability screens the Turing instability if the former precedes the latter instability in reaction-diffusion system. In Fig. 7(h) we can see as the Turing and Hopf instabilities appear simultaneously, both the reaction and diffusion entropy production rates are modified sufficiently from the initial zero value. Corresponding concentration profiles in all the cases are shown in the first row of Fig. 7.

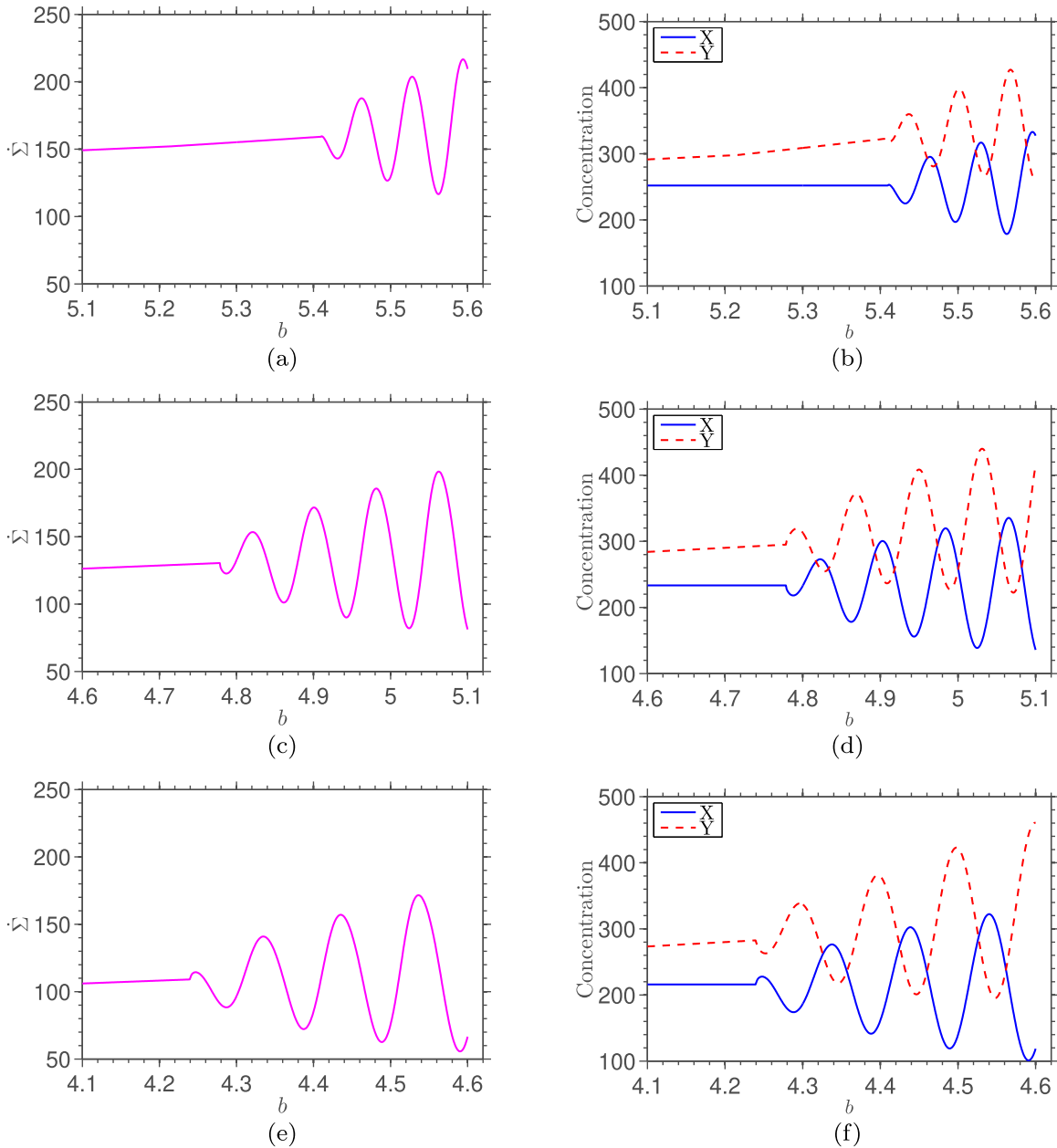


FIG. 6. Total entropy production (left column) as function of externally controlled parameter  $b$  calculated analytically for a 1D Brusselator model of length  $l = 9.5$  at time  $t = 150$  and absolute temperature  $T = 300$  K for three different values of parameter  $a$  leading to three different scenarios of Turing-Hopf interplay: [(a) and (b)] for  $a = 2.1$ , Turing first; [(c) and (d)] for COD2-Turing and Hopf that appear simultaneously; and [(e) and (f)] for  $a = 1.8$ , Hopf first. Total entropy production expressed as the sum of entropy production rates due to diffusion and reaction parts. Global concentration field of intermediate species  $X$  and  $Y$  as a function of  $b$  are shown in the right column. In all the three cases it is very apparent from the figures that entropy production rate is proportional to global concentration of  $X$  (or  $Y$ ). For all the cases diffusion coefficients are  $D_{11} = D_{22} = 1$ ,  $D_{12} = 0.51$ , and  $D_{21} = -0.51$  and reaction rate constants are  $K_{-\rho} = 10^{-4} \ll K_{\rho} = 1$ . (i.e., for the weakly reversible case).

The left column of Fig. 8 shows the semigrand Gibbs free-energy change as a function of chemical energy of the control parameter  $b$ . As suggested by Figs. 8(a), 8(c), and 8(e) for “Turing first,” “COD2” and “Hopf first,” respectively, the transformed Gibbs free energy of the unstable homogeneous part basically sets the baseline for the transformed Gibbs free energy corresponding to the part where pattern formation arises. This clearly suggests that the transformed Gibbs free energy plays the role of the proper nonequilibrium thermo-

dynamic potential of the reaction-diffusion system in the presence of Turing-Hopf interplay, at least in a global sense. A plot of the slopes for the same thermodynamic entity is shown in the right column of Fig. 8 to get a more clear idea about the phase transitions in the response of the thermodynamic entity for whether Turing [Fig. 8(b)] or Hopf instability [Fig. 8(f)] appears first or both of them appear simultaneously [Fig. 8(d)] as control parameter  $b$  is varied. In Figs. 7 and 8, due to Turing Hopf interplay one obtains oscillation in concentration

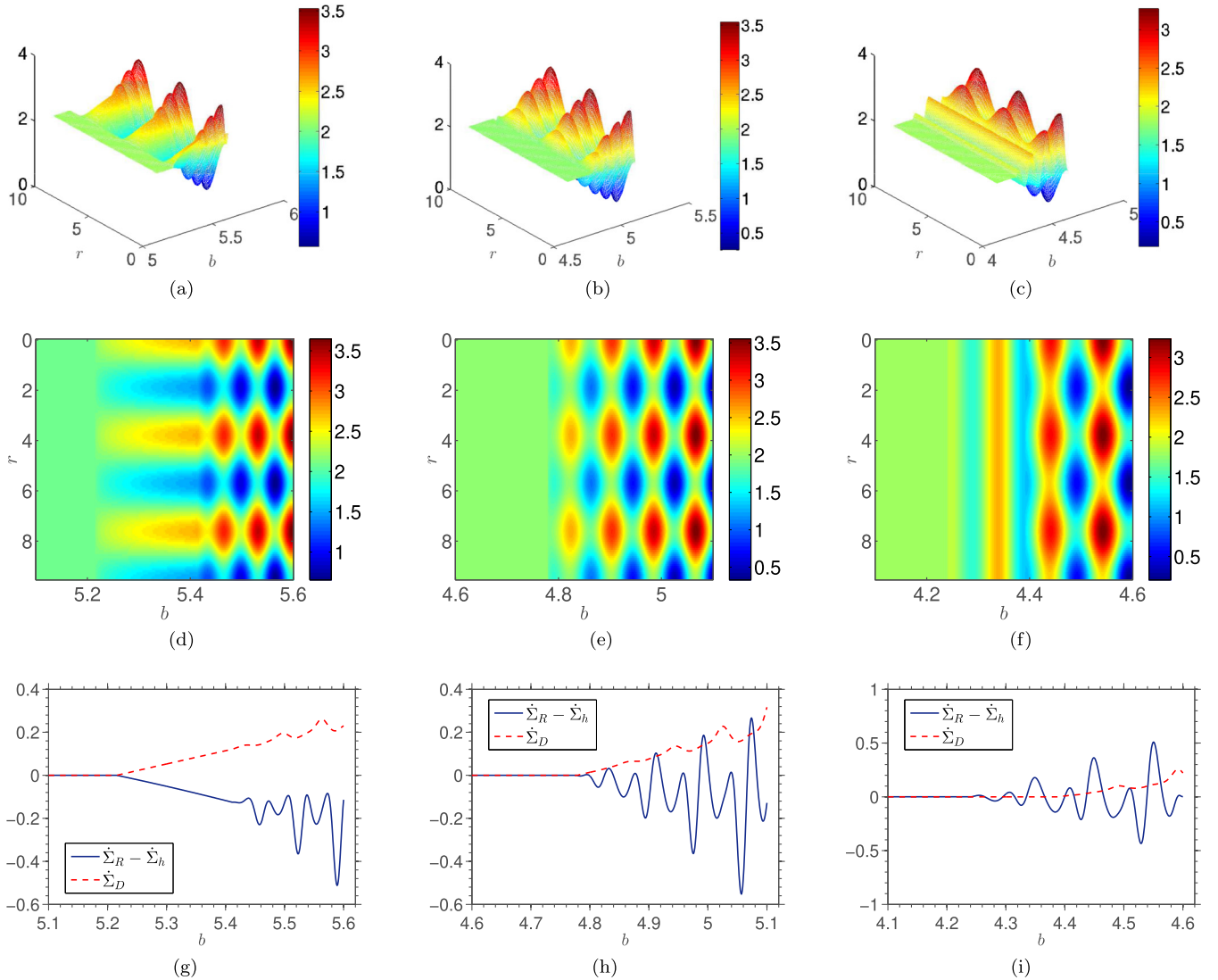


FIG. 7. In the first row, 3D concentration fields of  $X$  in the Brusselator model of length  $l = 9.5$  as a function of externally controlled parameter  $b$  at  $t = 150$  and  $T = 300$  K for three different values of parameter  $a$  leading to three different scenarios of Turing-Hopf interplay are shown (plots of  $Y$  are similar). Here a “jet” colormap is used to show contrast in concentration field. Figures of the second row shows image of these concentration fields of  $X$ . Extended spatial dimension is shown along the vertical axis. In the third row the corresponding analytical result of EPR for reaction ( $\dot{\Sigma}_R$ ) and diffusion ( $\dot{\Sigma}_D$ ) as function of control parameter  $b$  is presented. The solid blue lines corresponds to the difference between reaction part and the homogeneous part of the reaction-diffusion system and red dashed lines refer to the diffusion part of entropy production rate. [(a), (d), and (g)] For  $a = 2.1$ , Turing first; [(b), (e), and (h)] for COD2-Turing and Hopf appearing simultaneously; [(c), (f), and (i)] for  $a = 1.8$ , Hopf first.

and thermodynamic quantities with  $b$  and  $\mu_b$ . A series of phase transitions can open up the opportunity to control concentration and the free-energy profile both spatially and dynamically by varying the chemostatted species  $B$ .

## IX. CONCLUSIONS

In this work, we have investigated the energetic and entropic costs of pattern arising in the realm of Turing-Hopf interplay in a standard model system by determining proper nonequilibrium potential and entropy production rate in an open system with finite size. In a systematic way we have shown here how the concentration, nonequilibrium semigrand Gibbs free energy and entropy production rate at steady state

drastically depend on a control parameter in the Turing-Hopf interplay regime for three possible situations. This approach will also help to control and manipulate the efficiency and dissipation of a system far from equilibrium. It also paves the way to relate Turing-Hopf interplay with the instance of nonequilibrium phase transitions which generates a possibility of huge modulation of free-energy and concentration profiles. Here we capture as well as quantify the effect of diffusion on the Hopf limit cycle through the diffusion-driven Turing instability. Proportionality of total EPR with the global concentration profile is an important result in the context of the entropic cost of pattern formation and thus for the evolution of real chemical or biological systems in larger sense. Furthermore, we have found that these outcomes are also

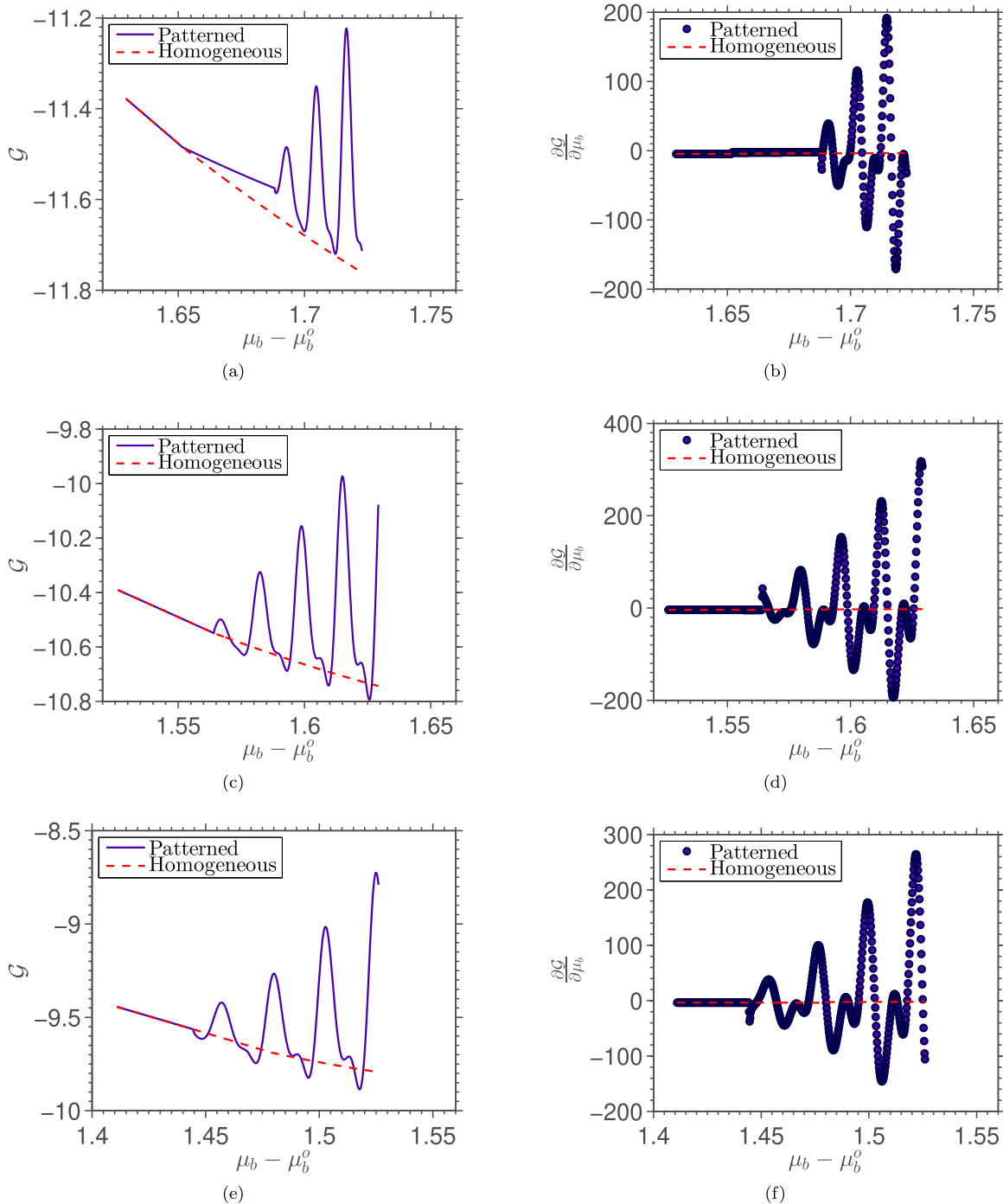


FIG. 8. Semigrand Gibbs free energy (left column) and corresponding slope (right column) profiles calculated analytically as function of chemical potential of control parameter  $b$  in 1D the Brusselator model at  $t = 150$  and  $T = 300$  K for three different values of parameter  $a$  leading to three different scenarios of Turing-Hopf interplay: [(a) and (b)] For  $a = 2.1$  Turing first; [(c) and (d)] for COD2 Turing and Hopf appearing simultaneously; and [(e) and (f)] for  $a = 1.8$ , Hopf first.  $A$  and  $B$  are considered as the reference chemostatted species to define nonequilibrium free energy in an open system. The dotted lines are for an unstable homogeneous state of the system with no pattern. For all the cases the diffusion coefficients are  $D_{11} = D_{22} = 1$ ,  $D_{12} = 0.51$ , and  $D_{21} = -0.51$  and reaction rate constants are  $K_{-\rho} = 10^{-4} \ll K_{\rho} = 1$ .

valid for the experimentally found magnitudes of the self- and cross-diffusion coefficients. The only thing that would be different for the experimental values of diffusion coefficients is the period of oscillations as the parameter  $a$ , on which critical frequency of the Hopf bifurcation depends, is shifted to a new value due to this different set of diffusion coefficients.

Amplitude equation formalism, a universal description in terms of dynamical symmetry breaking near a bifurcation point, has been utilized here to lay the basis of analytical construction. The approximate amplitude solution obtained by the analytical scheme for equal self-diffusion coefficients can describe the dynamical phenomena found in the experiments with high accuracy [49]. In our approach of finding

the amplitude equation by exploiting the KB scheme, we have considered both the self- and cross-diffusion coefficients which are generally not equal. In this aspect, our results related to the amplitude equation is more general and would be quite useful in the environment where cross diffusion is present.

It turns out that even in the absence of the “local activation and long-range inhibition” condition [9] with equal self-diffusion coefficients of the species, proper choice of cross-diffusion coefficients can lead to the diffusive instabilities as the mathematical expressions of the intrinsic critical values of control parameter as well as wave number explicitly contain cross-diffusion coefficients. So Turing instabilities considered here are essentially cross diffusion driven and this kind of thermodynamic description is valid beyond the traditional Turing pattern. Our selection of the Brusselator model in this study excludes the possibility of subcritical Hopf bifurcation. Here we have inspected weak Turing-Hopf interplay and have not

considered subharmonic oscillation in this kind of interplay. We believe this framework for Turing-Hopf interplay will also be applicable to study the thermodynamics of Turing-Hopf interaction in a superdiffusive two species model [60].

This analytically tractable thermodynamic description of the reaction-diffusion system is found to be powerful enough to capture almost all of the essential richness of the Turing-Hopf interaction in an open chemical network. In linear nonequilibrium thermodynamics, the thermodynamic driving force is specified as flux times Onsager coefficients near equilibrium. Here the reaction affinity for a system kept far from equilibrium is expressed directly from the elementary chemical reaction containing the nonlinear autocatalytic reaction. This approach of nonequilibrium thermodynamics on top of nonlinear dynamical features considered here for pattern formation could also be implemented in kinetic proofreading [61,62], enzyme-assisted copolymerization [63], and in several nonequilibrium steady states of biochemical systems [24].

- 
- [1] M. Cross and H. Greenside, *Pattern Formation and Dynamics in Nonequilibrium Systems* (Cambridge University Press, Cambridge, 2009).
- [2] A. M. Turing, The chemical basis of morphogenesis, *Philos. Trans. R. Soc. Lond. B* **237**, 37 (1952).
- [3] I. R. Epstein and J. A. Pojman, *An Introduction to Nonlinear Chemical Dynamics: Oscillations, Waves, Patterns, and Chaos* (Oxford University Press, Oxford, 1998).
- [4] V. Castets, E. Dulos, J. Boissonade, and P. De Kepper, Experimental Evidence of a Sustained Standing Turing-Type Nonequilibrium Chemical Pattern, *Phys. Rev. Lett.* **64**, 2953 (1990).
- [5] Q. Ouyang and H. L. Swinney, Transition from a uniform state to hexagonal and striped turing patterns, *Nature* **352**, 610 (1991).
- [6] A. Zaikin and A. Zhabotinsky, Concentration wave propagation in two-dimensional liquid-phase self-oscillating system, *Nature* **225**, 535 (1970).
- [7] A. T. Winfree, Spiral waves of chemical activity, *Science* **175**, 634 (1972).
- [8] A. M. Zhabotinsky, M. Dolnik, and I. R. Epstein, Pattern formation arising from wave instability in a simple reaction-diffusion system, *J. Chem. Phys.* **103**, 10306 (1995).
- [9] J. D. Murray, *Interdisciplinary Applied Mathematics* (Springer, Berlin, 2003), Vol. 2, p. 838.
- [10] S. Kondo and T. Miura, Reaction-diffusion model as a framework for understanding biological pattern formation, *Science* **329**, 1616 (2010).
- [11] D. Iber and D. Menshykau, The control of branching morphogenesis, *Open Biol.* **3**, 130088 (2013).
- [12] S. Kretschmer and P. Schwillie, Pattern formation on membranes and its role in bacterial cell division, *Curr. Opin. Cell Biol.* **38**, 52 (2016).
- [13] A. Goldbeter, *Biochemical Oscillations and Cellular Rhythms: The Molecular Bases of Periodic and Chaotic Behaviour* (Cambridge University Press, Cambridge, UK, 1997).
- [14] M. Falcke, Reading the patterns in living cells—the physics of  $Ca^{2+}$  signaling, *Adv. Phys.* **53**, 255 (2004).
- [15] K. Thurley, A. Skupin, R. Thul, and M. Falcke, Fundamental properties of  $Ca^{2+}$  signals, *Biochim. Biophys. Acta* **1820**, 1185 (2012).
- [16] D. Kondepudi and I. Prigogine, *Modern Thermodynamics* (John Wiley & Sons, Chichester, UK, 2014).
- [17] Y. Kuramoto, *Chemical Oscillations, Waves, and Turbulence*, Springer Series in Synergetics (Springer, Berlin, 1984), Vol. 19.
- [18] P. J. Ortoleva, *Geochemical Self-organization* (Clarendon Press, London, 1994).
- [19] N. Kumar and W. Horsthemke, Effects of cross diffusion on Turing bifurcations in two-species reaction-transport systems, *Phys. Rev. E* **83**, 036105 (2011).
- [20] E. P. Zemskov, K. Kassner, M. J. B. Hauser, and W. Horsthemke, Turing space in reaction-diffusion systems with density-dependent cross diffusion, *Phys. Rev. E* **87**, 032906 (2013).
- [21] Z. Lin, R. Ruiz-Baier, and C. Tian, Finite volume element approximation of an inhomogeneous brusselator model with cross-diffusion, *J. Comput. Phys.* **256**, 806 (2014).
- [22] I. Prigogine and R. Lefever, Symmetry breaking instabilities in dissipative systems. II, *J. Chem. Phys.* **48**, 1695 (1968).
- [23] G. Nicolis and I. I. Prigogine, *Self-organization in Nonequilibrium Systems: From Dissipative Structures to Order through Fluctuations* (Wiley, New York, 1977), p. 491.
- [24] H. Qian, Open-system nonequilibrium steady state: Statistical thermodynamics, fluctuations, and chemical oscillations, *J. Phys. Chem. B* **110**, 15063 (2006).
- [25] H. Qian, S. Kjelstrup, A. B. Kolomeisky, and D. Bedeaux, Entropy production in mesoscopic stochastic thermodynamics: Nonequilibrium kinetic cycles driven by chemical potentials, temperatures, and mechanical forces, *J. Phys.: Condens. Matter* **28**, 153004 (2016).
- [26] C. Van den Broeck and K. Lindenberg, Efficiency at maximum power for classical particle transport, *Phys. Rev. E* **86**, 041144 (2012).



- [27] K. Proesmans, B. Cleuren, and C. V. den Broeck, Stochastic efficiency for effusion as a thermal engine, *Europhys. Lett.* **109**, 20004 (2015).
- [28] D. Collin, F. Ritort, C. Jarzynski, S. B. Smith, I. Tinoco Jr, and C. Bustamante, Verification of the crooks fluctuation theorem and recovery of rna folding free energies, *Nature* **437**, 231 (2005).
- [29] G. Hummer and A. Szabo, Free energy reconstruction from nonequilibrium single-molecule pulling experiments, *Proc. Natl. Acad. Sci. USA* **98**, 3658 (2001).
- [30] M. Polettini and M. Esposito, Irreversible thermodynamics of open chemical networks. I. Emergent cycles and broken conservation laws, *J. Chem. Phys.* **141**, 024117 (2014).
- [31] R. Rao and M. Esposito, Nonequilibrium Thermodynamics of Chemical Reaction Networks: Wisdom from Stochastic Thermodynamics, *Phys. Rev. X* **6**, 041064 (2016).
- [32] R. A. Alberty, *Thermodynamics of Biochemical Reactions* (John Wiley & Sons, Hoboken, NJ, 2003).
- [33] I. S. Aranson and L. Kramer, The world of the complex ginzburg-landau equation, *Rev. Mod. Phys.* **74**, 99 (2002).
- [34] D. Walgraef, The hopf bifurcation and related spatio-temporal patterns, in *Spatio-Temporal Pattern Formation* (Springer, Berlin, 1997), pp. 65–85.
- [35] G. Falasco, R. Rao, and M. Esposito, Information Thermodynamics of Turing Patterns, *Phys. Rev. Lett.* **121**, 108301 (2018).
- [36] F. Avanzini, G. Falasco, and M. Esposito, Thermodynamics of chemical waves, *J. Chem. Phys.* **151**, 234103 (2019).
- [37] A. De Wit, D. Lima, G. Dewel, and P. Borckmans, Spatiotemporal dynamics near a codimension-two point, *Phys. Rev. E* **54**, 261 (1996).
- [38] W. Just, M. Bose, S. Bose, H. Engel, and E. Schöll, Spatiotemporal dynamics near a supercritical turing-hopf bifurcation in a two-dimensional reaction-diffusion system, *Phys. Rev. E* **64**, 026219 (2001).
- [39] L. Yang and I. R. Epstein, Oscillatory Turing Patterns in Reaction-Diffusion Systems with Two Coupled Layers, *Phys. Rev. Lett.* **90**, 178303 (2003).
- [40] M. R. Ricard and S. Mischler, Turing instabilities at hopf bifurcation, *J. Nonlinear Sci.* **19**, 467 (2009).
- [41] V. K. Vanag and I. R. Epstein, Cross-diffusion and pattern formation in reaction-diffusion systems, *Phys. Chem. Chem. Phys.* **11**, 897 (2009).
- [42] N. M. Krylov and N. N. Bogoliubov, *Introduction to Non-linear Mechanics* (Princeton University Press, Princeton, NJ, 1949).
- [43] A. M. Zhabotinsky, A history of chemical oscillations and waves, *Chaos* **1**, 379 (1991).
- [44] J. M. Chung and E. Peacock-López, Bifurcation diagrams and turing patterns in a chemical self-replicating reaction-diffusion system with cross diffusion, *J. Chem. Phys.* **127**, 174903 (2007).
- [45] R. J. Field, E. Koros, and R. M. Noyes, Oscillations in chemical systems. ii. Thorough analysis of temporal oscillation in the bromate-cerium-malonic acid system, *J. Am. Chem. Soc.* **94**, 8649 (1972).
- [46] R. J. Field and R. M. Noyes, Oscillations in chemical systems. iv. Limit cycle behavior in a model of a real chemical reaction, *J. Chem. Phys.* **60**, 1877 (1974).
- [47] A. I. Lavrova, E. B. Postnikov, and Y. M. Romanovsky, Brusselator—An abstract chemical reaction?, *Phys. Usp.* **52**, 1239 (2009).
- [48] J. W. S. Rayleigh and R. B. Lindsay, *The Theory of Sound* (Dover, London, 1945).
- [49] A. I. Lavrova, L. Schimansky-Geier, and E. B. Postnikov, Phase reversal in the Selkov model with inhomogeneous influx, *Phys. Rev. E* **79**, 057102 (2009).
- [50] G. Nicolis, *Introduction to Nonlinear Science* (Cambridge University Press, Cambridge, UK, 1995) p. 254.
- [51] E. P. Zemskov, V. K. Vanag, and I. R. Epstein, Amplitude equations for reaction-diffusion systems with cross diffusion, *Phys. Rev. E* **84**, 036216 (2011).
- [52] I. Prigogine, *Chemical Thermodynamics [by] I. Prigogine and R. Defay* (Longmans, London, 1954).
- [53] E. Fermi, *Thermodynamics* (Dover, London, 1956), p. 160.
- [54] T. M. Cover and J. A. Thomas, *Elements of Information Theory* (Wiley-India, New Delhi 1999), p. 542.
- [55] V. K. Vanag, F. Rossi, A. Cherkashin, and I. R. Epstein, Cross-diffusion in a water-in-oil microemulsion loaded with malonic acid or ferroin. taylor dispersion method for four-component systems, *J. Phys. Chem. B* **112**, 9058 (2008).
- [56] F. Rossi, V. K. Vanag, E. Tiezzi, and I. R. Epstein, Quaternary cross-diffusion in water-in-oil microemulsions loaded with a component of the belousov-zhabotinsky reaction, *J. Phys. Chem. B* **114**, 8140 (2010).
- [57] F. Rossi, V. K. Vanag, and I. R. Epstein, Pentanary cross-diffusion in water-in-oil microemulsions loaded with two components of the belousov-zhabotinsky reaction, *Chem. Eur. J.* **17**, 2138 (2011).
- [58] V. K. Vanag and I. R. Epstein, Segmented spiral waves in a reaction-diffusion system, *Proc. Natl. Acad. Sci. USA* **100**, 14635 (2003).
- [59] I. R. Epstein and V. K. Vanag, Complex patterns in reactive microemulsions: Self-organized nanostructures?, *Chaos* **15**, 047510 (2005).
- [60] J. Tzou, B. Matkowsky, and V. Volpert, Interaction of Turing and Hopf modes in the superdiffusive Brusselator model, *Appl. Math. Lett.* **22**, 1432 (2009).
- [61] J. J. Hopfield, R. Peterson, and S. Spiegelman, Kinetic proof-reading: A new mechanism for reducing errors in biosynthetic processes requiring high specificity, *Proc. Natl. Acad. Sci. USA* **71**, 4135 (1974).
- [62] H. Ge, M. Qian, and H. Qian, Stochastic theory of nonequilibrium steady states. Part II: Applications in chemical biophysics, *Phys. Rep.* **510**, 87 (2012).
- [63] D. Andrieux and P. Gaspard, Nonequilibrium generation of information in copolymerization processes, *Proc. Natl. Acad. Sci. USA* **105**, 9516 (2008).